A comprehensive approach for the simulation of the Urban Heat Island effect with the WRF/SLUCM modeling system: The case of Athens (Greece)

Christos Giannaros[a,*], Athanasios Nenes[b,c,d,e], Theodore M. Giannaros[e], Konstantinos Kourtidis[f], Dimitrios Melas[a]

[a] Laboratory of Atmospheric Physics, Aristotle University of Thessaloniki, PO Box 149, 54124 Thessaloniki, Greece
[b] School of Earth and Atmospheric Sciences, Georgia Institute of Technology, Atlanta, GA 30332-0340, USA
[c] School of Chemical and Biomolecular Engineering, Georgia Institute of Technology, Atlanta, GA 30332-0100, USA
[d] Institute of Chemical Engineering Sciences, Foundation for Research and Technology, Hellas, 26504 Patras, Greece
[e] Institute for Environmental Research and Sustainable Development, National Observatory of Athens, Vas. Pavlou & I. Metaxa, 15236 Penteli, Greece
[f] Laboratory of Atmospheric Pollution and Pollution Control Engineering of Atmospheric Pollutants, Department of Environmental Engineering, Democritus University of Thrace, 67100 Xanthi, Greece

ARTICLE INFO

ABSTRACT

This study presents a comprehensive modeling approach for simulating the spatiotemporal distribution of urban air temperatures with a modeling system that includes the Weather Research and Forecasting (WRF) model and the Single-Layer Urban Canopy Model (SLUCM) with a modified treatment of the impervious surface temperature. The model was applied to simulate a 3-day summer heat wave event over the city of Athens, Greece. The simulation, using default SLUCM parameters, is capable of capturing the observed diurnal variation of urban temperatures and the Urban Heat Island (UHI) in the greater Athens Area (GAA), albeit with systematic biases that are prominent during nighttime hours. These biases are particularly evident over low-intensity residential areas, and they are associated with the surface and urban canopy properties representing the urban environment. A series of sensitivity simulations unravels the importance of the sub-grid urban fraction parameter, surface albedo, and street canyon geometry in the overall causation and development of the UHI effect. The sensitivities are then used to determine optimal values of the street canyon geometry, which reproduces the observed temperatures throughout the simulation domain. The optimal parameters, apart from considerably improving model performance (reductions in mean temperature bias from 0.30 °C to 1.58 °C), are also consistent with actual city building characteristics – which gives confidence that the model set-up is robust, and can be used to study the UHI in the GAA in the anticipated warmer conditions in the future.

1. Introduction

Urban expansion is accelerating worldwide and results in the replacement of green and natural surfaces by human-made structures and roads. These constructions fundamentally alter land-surface characteristics, which in turn modifies the surface energy budget (SEB) and land-atmosphere interactions (Loupa et al., 2016). The urban heat island (UHI) effect, referred to the excess warmth of cities compared to the surrounding non-urbanized territories (Arnfield, 2003; Christen and Vogt, 2004; Giannaros et al., 2014; Kourtidis et al., 2015; Peng et al., 2012; Sismanidis et al., 2015), is perhaps the most representative environmental problem arising from local climate modifications due to urbanization (Georgescu et al., 2014; Oke, 1982, 1987; Santamouris, 2007; Ward et al., 2016; Zhao et al., 2014). A considerable body of

research shows that UHIs interact synergistically with heat wave (HW) events exacerbating their effect on urban residents (e.g., Li and Bou-Zeid, 2013; Tan et al., 2010), and as a result heat-related death risk under exceptional hot weather conditions in urban environments is much higher than in the rural surroundings (Conti et al., 2005; Heaviside et al., 2016; Gabriel and Endlicher, 2011). UHI effects become even more important when considering that in a changing climate, the frequency of HWs will increase together with their intensity and duration (e.g., Beniston, 2004; Founda and Giannakopoulos, 2009; Meehl and Tebaldi, 2004). Furthermore, > 50% of the world population is living in urban areas, with a projected 60% (66.4%) by 2030 (2050) worldwide (United Nations, 2014). The combined effects of rapid urbanization, global warming, and UHIs are expected to make the urban residents more vulnerable to the adverse health impacts arising

---

from extreme heat conditions. However, not every mega city and urban environment is equally susceptible to these changes. Therefore a rational approach is required to adapt each urban population to thermal stress and develop specific mitigation strategies to minimize associated risks.

Numerical models can be a valuable tool in this direction due to their ability to provide detailed spatiotemporal information on UHI effect regarding attribution, operational forecasting, future climate projection, and investigation of mitigation scenarios. Extensive research over the past decade contributed significantly to a better understanding and representation of the processes involved in the formation of UHI through the application of mesoscale numerical weather prediction (NWP) models. The parameterizations of urban effects in meteorological models follow two main approaches (Kusaka et al., 2001): (a) a modified surface energy balance through improved soil and surface characteristics (e.g. surface albedo) to better represent urban areas (Giannaros et al., 2013; Liu et al., 2006; Miao et al., 2007), and (b) a coupling with an urban canopy model that considers the street canyon geometry for describing in more detail the sub-grid scale atmospheric dynamics and thermodynamics in cities (Best, 2005; Dupont et al., 2004; Martilli, 2002; Hamdi and Schayes, 2008). Both approaches require the specification of surface parameters, while urban canopy properties (UCPs) are necessary for the realistic representation of urban morphology in the second method. Such data are unique for each city, and remote sensing and GIS techniques (e.g. Ching et al., 2009) have been utilized for the acquisition of them. However, the availability of them is limited to few geographical areas and, hence, alternative methods need to be addressed. Additionally, the identification of how each surface parameter and UCP operates and contributes to the diurnal temperature response is very crucial for the faithful replication of UHI effect, especially during HW event periods.

Despite previous substantial efforts and progress on the predictive understanding of UHI, the above challenges in implementing reliable UHI modeling systems remain open, especially for the East Mediterranean, which is one of the most vulnerable areas regarding climate change. For this, the present study aims to provide a comprehensive approach for constraining, studying and simulating urban temperatures (and UHI effect) with the Weather Research and Forecasting (WRF) model coupled with an urban canopy model (Li and Bou-Zeid, 2014; Meng et al., 2011; Salamanca et al., 2012; Vahmani and Ban-Weiss, 2016; Chen et al., 2014). The performance of WRF under different urban parameterizations and code modifications was evaluated over the greater Athens area (GAA), Greece. We systematically explore the sensitivity of the model response to highly uncertain land surface and urban canopy properties, which subsequently were used to define an optimal set of parameters and model configuration that best reproduced the temperature distributions measured during a 3-day HW episode (July 24–July 26, 2009) that occurred over the E. Mediterranean and strongly affected the GAA.

2. Methodology

2.1. Area of interest and data sources

The study area is Athens, the capital and largest city of Greece. The greater Athens area (GAA) covers 450 km^2, and the built-up zone extends throughout the central plain of a basin known as the Attica Basin. The city of Athens is characterized by a complex geomorphology as it is bounded by four high mountains (Mount Parnitha to the north, Mount Penteli to the northeast, Mount Aigaleo to the west and Mount Hymettus to east), and it is open to the sea (Saronic Gulf) from the southwest (Fig. 1a). High-intensity residential areas are located in the core of the city, while the suburbs include built-up areas (e.g. Helliniko airport) and low-intensity residential (Fig. 1b). The main industrial zone of Athens is located in Elefsina at the northwest part of the basin (Fig. 1a–b).

Athens has a typical Mediterranean climate, characterized by warm and dry summers with July and August being the hottest months. An important climatic feature in the GAA is the increasing frequency, intensity, and duration of heat wave episodes (Founda et al., 2004), during which peak daytime temperatures can exceed 37 °C (e.g., 46 °C in the summer of 2007; Kourtidis et al., 2015). Heat waves are often accompanied by severe air quality episodes, given that both occur under conditions of high insolation and stagnation which strongly promotes the levels of photochemical pollution and levels of Saharan dust (Papanastasiou et al., 2010, 2015), giving average daily concentrations of O_3 and particulate matter that exceed 120 $\mu g/m^3$ and 50 $\mu g/m^3$, respectively.

Understanding the extent of UHI effects on urban temperatures throughout the GAA requires a careful characterization of surface properties, building structures and spatially distributions of temperature during HW episodes. This was the focus of the THERMOPOLIS 2009 campaign (Daglis et al., 2010a, 2010b), when satellite, airborne and ground-based observations between July 15 and July 31, 2009, were combined to characterize the UHI of Athens. Of the data collected, we focus on near-surface air temperature measurements from 19 ground-based stations operated by the Democritus University of Thrace (DUTH), the National Observatory of Athens (NOA), the Hellenic National Meteorological Service (HNMS) and the National and Technical University of Athens (NTUA). The characteristics of each observational site are listed in Table 1, while the locations of the sites are shown in Fig. 1b.

2.2. Urbanization in the WRF modeling framework

The modeling system used in the current study is the WRF, version 3.5.1 (Skamarock et al., 2008) coupled with Noah land surface model (LSM) (Tewari et al., 2004) that represents land-atmosphere interactions through heat, momentum and moisture fluxes. The Noah LSM treats urban areas as homogeneous, flat surfaces with properly modified thermal, radiative, moisture and aerodynamic properties to account for the urban effects. The enhancements of the urban surface properties in the Noah LSM include: (a) a decreased green vegetation fraction (GVF) of 0.05 to reduce evaporation, (b) a reduction of surface albedo to 0.15 to represent the enhanced absorption of short-wave radiation, (c) a reduced surface emissivity to 0.88 to decrease nocturnal radiative cooling, and (d) an increased surface roughness length of 0.50 m to parametrize the strengthened drag and blocking effects. This is the standard approach used for the urbanization of the WRF and is referred as the bulk urban parameterization (Liu et al., 2006).

A more detailed treatment of the urban environment in the WRF/ Noah modeling system requires its coupling with an urban canopy model. An urban canopy model includes the effects of urban geomorphology on the dynamic, radiation and thermodynamic processes at the model sub-grid scale. Such an approach requires precise urban land use data and parameters that represent the canopy geometry, where the urban fraction (F_{urb}) parameter defines the percentage of the impervious to water surfaces (e.g. buildings) in the WRF sub-grid proportion (Chen et al., 2011). The single-layer urban canopy model (SLUCM) by Kusaka et al. (2001) and Kusaka and Kimura (2004) distinguishes three types of urban surface: (i) low-intensity residential (LIR), (ii) high-intensity residential (HIR), and (iii) industrial/commercial (IC), each of which can contain ground, wall, and roof facets. For a given urban grid cell that is dominated by LIR, 50% (F_{urb} = 0.50) of the grid cell is covered by the impervious urban facets, while the remaining fraction is treated as a pervious, vegetated surface. The corresponding percentages for urban grid cells that characterized as HIR and IC, are 90% (F_{urb} = 0.90) and 95% (F_{urb} = 0.95), respectively (Chen et al., 2011).

In the current modeling framework, the Noah LSM is first called to compute the surface fluxes and land surface temperature (LST) for the grass-covered part; the SLUCM is then called to calculate the LST and
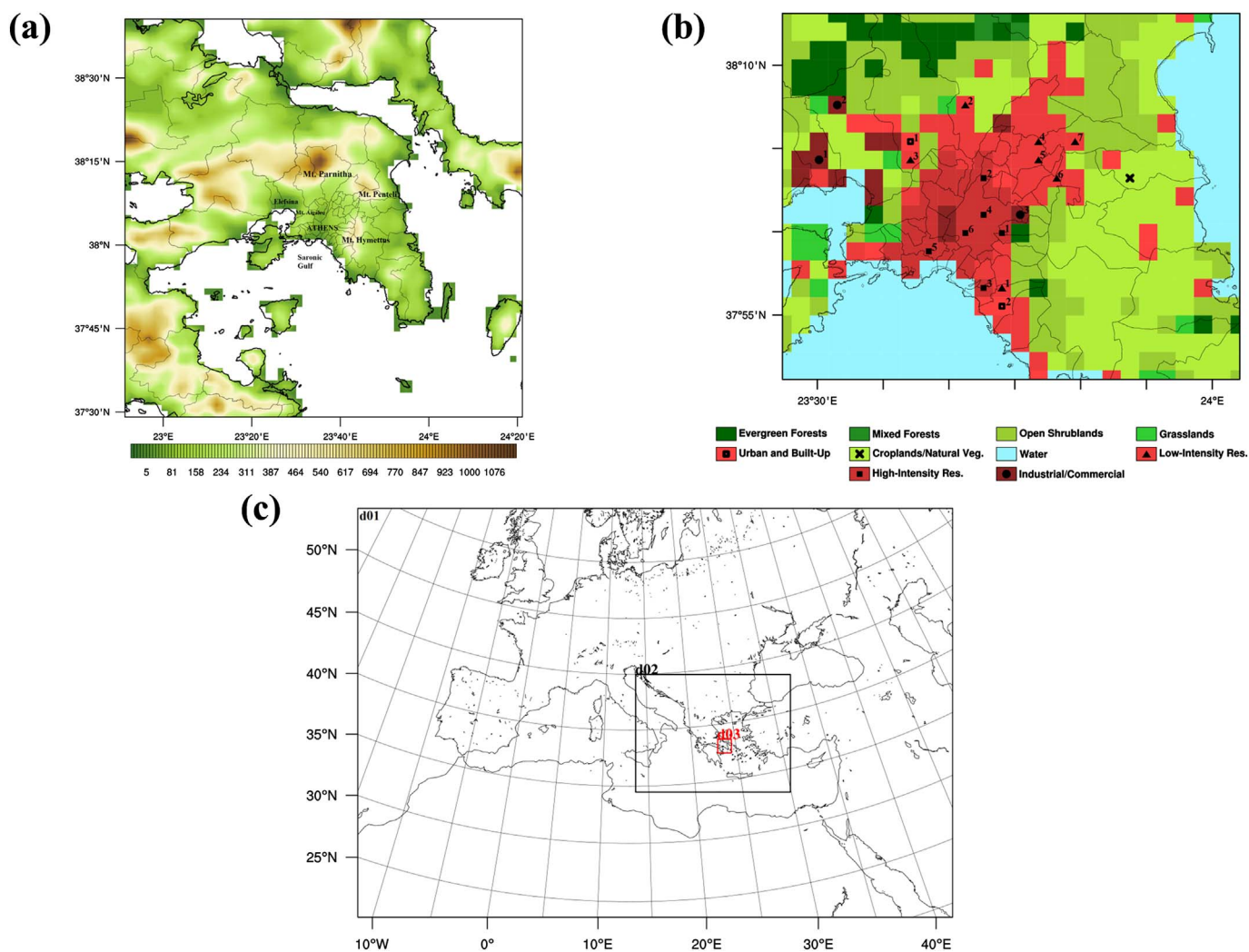
Fig. 1. (a) Topography of GAA with identification of the main geomorphological features. (b) Land use (CORINE dataset) and locations of the ground-based measurement sites. (c) Three 2-way nested WRF modeling domains (Lambert Conformal Projection).

Table 1
Summary of the characteristics of the 19 ground-based measurement sites.

Station ID	Monitoring network	Station name	Latitude (°N)	Longitude (°E)	Altitude(m a.s.l.[a])	Land use classification
LIR-1	NTUA	Ilioupoli	37.92	23.76	206	Low intensity residential
LIR-2	NTUA	Menidi	38.11	23.73	210	Low intensity residential
LIR-3	HNMS	Nea Filadelfia	38.05	23.66	245	Low Intensity Residential
LIR-4	DUTH	Papayannis	38.06	23.81	235	Low intensity residential
LIR-5	DUTH	Pellis	38.03	23.82	211	Low intensity residential
LIR-6	NOA	Penteli	38.05	23.87	495	Low intensity residential
LIR-7	DUTH	Thalias	38.02	23.83	217	Low intensity residential
HIR-1	DUTH	Anaximenous	37.97	23.75	125	High intensity residential
HIR-2	NTUA	Galatsi	38.03	23.76	176	High intensity residential
HIR-3	DUTH	Kountouriotou	37.93	23.71	29	High intensity residential
HIR-4	DUTH	Pipinou	38.00	23.73	101	High intensity residential
HIR-5	DUTH	Serifou	37.96	23.66	8	High intensity residential
HIR-6	NOA	Thisio	37.97	23.72	95	High intensity residential
UB-1	NTUA	Ano Liosia	38.08	23.67	184	Urban and built-up
UB-2	NTUA	Helliniko	37.90	23.74	6	Urban and built-up
IC-1	HNMS	Elefsina	38.07	23.55	30	Industrial/commercial
IC-2	NTUA	Mandra	38.12	23.56	258	Industrial/commercial
IC-3	NTUA	Zografou	37.98	23.79	181	Industrial/commercial
NVM	NTUA	Pikermi	38.00	23.93	133	Croplands/natural vegetation mosaic

[a] Above sea level.

surface fluxes over the impervious region. By default, the land surface characteristics for the pervious part of the urban grid cells correspond to that of the "croplands/natural vegetation mosaic" land use type, with an unvarying GVF of 0.8, a surface albedo of 0.18, emissivity of 0.98, and roughness length equal to 0.14 m (Vahmani and Ban-Weiss, 2016). Application of the SLUCM does not consider a GVF for the impervious part of the urban grid cell but requires 20 urban canopy parameters (UCPs) for each urban class type (LIR, HIR, IC) that are specified in a look-up table (URBPARM.TBL; Chen et al., 2011). Among these parameters are F_{urb}, mean building heights, roof and road widths, albedo and emissivity for the ground, the building walls, and roofs. The default albedo of ground, building walls and roofs s is 0.20, while the default emissivity of the ground is 0.95, and of walls and roofs is 0.90. Concerning the parameterization of roughness length, the SLUCM calculates three relevant parameters: (i) the canyon aerodynamic roughness length ($z0_c$), (ii) the canyon thermal roughness length ($z0_t$), and (iii) the roof aerodynamic roughness length ($z0_r$), using the semi-empirical formulations of Macdonald et al. (1998) – which in turn require the mean building height, the roof and road widths, and the standard deviation of roof height (i.e. building height variability).

The ultimate goal for UHI and HW impacts is to calculate the near-surface air temperature (SAT), defined at 2 m above ground level. SAT is a WRF diagnostic variable, interpolated between the lowest model layer height and surface (Shin and Hong, 2011) and calculated using an alternative expression of the sensible heat flux that uses atmospheric variables at 2 m (Li and Bou-Zeid, 2014):

$$SAT = LST - \frac{SH}{\rho C_{h2} U_2} \tag{1}$$

where SH is the total urban grid-scale sensible heat flux, ρ is the air density (kg/m^3), C_{h2} is the turbulent heat transfer coefficient at 2 m, and U_2 is the wind speed at 2 m.

The LST of an urban grid cell is computed as the weighted average of the impervious LST (LST_{urb}) and natural vegetated LST (LST_{veg}):

$$LST = F_{urb} LST_{urb} + (1 - F_{urb}) LST_{veg} \tag{2}$$

Likewise, SH is also weighted by the respective areal coverage:

$$SH = F_{urb} SH_{urb} + (1 - F_{urb}) SH_{veg} \tag{3}$$

where SH_{urb} is the sensible heat flux calculated by SLUCM for the impervious surfaces and SH_{veg} is the sensible heat flux from Noah LSM for the pervious surface. It is worth mentioning that the LST_{veg} is calculated as a prognostic variable by the Noah LSM using the properties of grasslands, while the LST_{urb} is generated as a diagnostic variable by the SLUCM following:

$$LST_{urb} = T_A - \frac{SH_{urb}}{\rho C_h U} \tag{4}$$

where T_A is the air temperature at the first level of the model, C_h the turbulent transfer coefficient, and U is the wind speed that corresponds to the first atmospheric layer of the model (Li and Bou-Zeid, 2014). T_A, C_h, and U are all WRF-derived prognostic variables.

Li and Bou-Zeid (2014) reported an inconsistency in the computation of the impervious surface temperature (Eq. (4)) which lead to significant biases in the simulated urban surface temperatures (Eq. (2)) which in turn contribute to errors in the calculation of the SAT (Eq. (1)). The problem is related to the turbulent transfer coefficient C_h for the whole urban grid cell which is inaccurately calculated using only the momentum and thermal roughness lengths of the grass-covered surface portion. To remove these errors, Li and Bou-Zeid (2014) proposed a revised calculation of LST_{urb} based on the prognostically-computed temperatures of the roof surfaces (T_{roof}) and the canyon (T_{canyon}):

$$LST_{urb} = F_{roof} T_{roof} + (1 - F_{roof}) T_{canyon} \tag{5}$$

where F_{roof} is the roof fraction of the impervious surface, i.e. plan area index, which is calculated as:

$$F_{roof} = \frac{W_{roof}}{W_{roof} + W_{road}} \tag{6}$$

where W_{roof} and W_{road} are the width of the roof and the road, respectively.

The C_{h2} used in the Eq. (1) is also calculated using only the thermal and momentum properties over grass. However, the SAT is much less sensitive to the turbulent transfer coefficient than the LST (Li and Bou-Zeid, 2014) and is considered a reliable diagnostic variable that can be used for the simulation of urban air temperatures as well as for the estimation of the canopy layer UHI.

2.3. Numerical simulations and experimental design

2.3.1. Model set-up

Fig. 1c shows the WRF domain configuration used in the present study. The model was applied over three 2-way nested modeling domains with horizontal grid resolutions of 18 km (d01), 6 km (d02) and 2 km (d03). The largest domain (d01) covers most of Europe and North Africa, d02 includes the E. Mediterranean and Balkan Peninsula, and, d03 focuses on the GAA. Each domain has 28 unevenly spaced full sigma layers in the vertical direction with the model top defined at 100 hPa.

The WRF simulations were initialized and forced at its lateral boundaries with the operational atmospheric analysis surface and pressure level data of the European Centre for Medium-range Weather Forecasts (ECMWF), provided at 0.25° × 0.25° spatial and 6 h temporal resolution. All simulations were conducted from 1200 UTC on July 23 to 0000 UTC 27 on July 27, 2009, with an output frequency of 1 h. The first 12 simulated hours were treated as spin-up period, while the remaining 72 h represented the 3-day heat wave episode over the city of Athens. The identification of the heat wave was based on IPCC's definition of extreme temperature index, TX90p (IPCC, 2013), according to which a warm day is determined when the daily maximum temperature exceeds the 90th percentile of the late-20th century period 1961–1990 (Giannaros et al., 2017).

The land use/land cover (LULC) data for domains 1 and 2 were taken from the 20-category and 30-arc-sec spatial resolution modified moderate resolution imaging spectroradiometer/international geosphere-biosphere project (MODIS-IGBP) global data. The MODIS-IGBP dataset includes only a single category (urban and built-up, UB) for representing urban areas and, thus, is considered to be inadequate for urban modeling applications, despite its relatively high horizontal resolution (~1 km). A more accurate urban LULC representation over the d03 domain is obtained from the 250 m spatial resolution European Environment Agency (EEA) CORINE land use data set (version 12/2009), remapped to the corresponding MODIS-IGBP LULC categories (Giannaros et al., 2014; Supplementary material Table S1). The CORINE LULC enables the three additional urban categories (HIR, LIR, IC), which are necessary for the implementation of SLUCM. Fig. 1b highlights the land use over the GAA according to the CORINE LULC data set.

The physical parameterization schemes applied in all domains include: (a) the WRF single-moment six-class scheme for handling the microphysics processes (Hong and Lim, 2006), (b) the asymmetric convection model 2 (ACM2) scheme for the planetary boundary layer (Pleim, 2007), (c) the revised MM5 scheme for parameterizing the model surface layer (Jiménez et al., 2012), (d) the Noah LSM (Tewari et al., 2004) for the land surface processes, (e) the Eta geophysical fluid dynamics laboratory (GFDL) scheme (Schwarzkopf and Fels, 1991), and the Dudhia scheme (Dudhia, 1989) for the longwave and shortwave radiation, respectively. Cumulus parameterization was used only for d01 and d02 by employing the Kain-Fritch scheme (Kain, 2004). The urban parameterization options are presented in the next section (Section 2.3.2).

Table 2
Summary of simulations.

Scenario	Urban parameterization	Modified model code for SLUCM	Albedo	Emissivity	Mean building height	Road width	Urban fraction
BUL	Bulk	–					
UCD	Single-Layer Urban Canopy Model (SLUCM)	–	–	–	–	–	–
UCM	Single-Layer Urban Canopy Model (SLUCM)	×	–	–	–	–	–
UCM_SAL	Single-Layer Urban Canopy Model (SLUCM)	×	×	–	–	–	–
UCM_SEM	Single-Layer Urban Canopy Model (SLUCM)	×	–	×	–	–	–
UCM_SBH	Single-Layer Urban Canopy Model (SLUCM)	×	–	–	×	–	–
UCM_SRW	Single-Layer Urban Canopy Model (SLUCM)	×	–	–	–	×	–
UCM_SUF	Single-Layer Urban Canopy Model (SLUCM)	×	–	–	–	–	×
UCM_OPT	Single-Layer Urban Canopy Model (SLUCM)	×	×	×	×	×	×

2.3.2. Design of the numerical experiments

A series of nine simulations were carried out in the present work (Table 2). The three first experiments, namely BUL, UCD, and UCM, were implemented to investigate the performance of the WRF model under different urban parameterization approaches. In the BUL simulation, the bulk urban parameterization of WRF/Noah modeling system was used. During the UCD scenario, the default SLUCM was utilized for the domain that covers the study area (d03), while the code of SLUCM was modified for the UCM experiment in order the impervious surface temperature (LST$_{urb}$; Eq. (5)) to be computed as proposed by Li and Bou-Zeid (2014). It is worth mentioning that when an urban grid cell is classified as UB, then the SLUCM corresponds this grid cell to the HIR type, concerning its tabulated UCPs. Table 3 shows the values of those characteristics that are subject to the current work. To ensure consistency during the evaluation and sensitivity analysis processes, the surface albedo and emissivity of SLUCM simulations were set equal to those of BUL scenario. For this, the SLUCM code was modified to assign the same values of albedo and emissivity to both pervious and impervious parts, including the three urban facets (roads, walls, roofs), of each urban grid cell. Another minor change concerns the building height variability, which was set equal to 3 m (= 1-floor height; www.statistics.gr) for all urban LULC types, to be representative for the city of Athens. Moreover, it should be noted that the SLUCM provides a default anthropogenic heating (AH) diurnal profile, which is user-editable, per urban LULC category (Sailor et al., 2015) to be added to the urban sensible heat flux term. However, there is a lack of AH databases for the city of Athens, as well as for many other cities, due to the high uncertainty in the specification of the AH spatial and temporal variability (Sailor and Lu, 2004). For this, in the current study, the AH model option was set off.

The UCM simulation was used as the base case scenario for conducting the sensitivity analysis to five critical surface and urban geometry properties. In the UCM_SAL experiment, the surface albedo of urban grid cells was reduced, while the surface emissivity was increased during the UCM_SEM simulation. These parameters are marked with high importance in the UHI causation and development. The specification of their values per urban LUCL category is highlighted in Table 3 and was based on the satellite-retrieved data (Giannaros et al., 2014) collected in the framework of the "UHI-UT" project funded by ESA. During the UCM_SBH, UCM_SRW and UCM_SUF scenarios, the mean building height, the road width and the urban fraction were reduced by 50%, respectively (Table 3). The building height and road width are of great importance in representing the complex geometry of street canyons, while interventions on urban fraction by increasing the remainder urban grass-covered portion (e.g. urban parks) can affect the local environment beneficially through the reduction of the UHI effect.

During the UCM_OPT simulation, the values of the examined surface and urban canopy properties were calibrated based on the sensitivity analysis, to be representative of the city of Athens and, consequently, lead to more adequate model SAT results. In particular, the land surface albedo and emissivity were replaced by the satellite remotely sensed data acquired during the "UHI-UT" project (Table 3), as several studies

pointed out that the utilization of satellite-derived land surface parameters improves the performance of NWP models (Ban-Weiss et al., 2015a, 2015b; Vahmani and Hogue, 2014; Vahmani and Ban-Weiss, 2016). The mean building height of LIR and HIR LULC class was increased by 80% and 100%, respectively, while it was decreased for IC LULC type by 40%. The road width parameter was not altered over IC sites, while it was raised from 8.3 m to 10 m and from 9.4 to 12 m over LIR and HIR areas, respectively. Finally, the urban fraction of LIR sites was increased to 80% (Table 3). These values of UCPs are close to those reported and used in other studies focusing on the urban area of GAA (Papangelis et al., 2012; Salvati et al., 2013; Shashua-Bar et al., 2010; Stathopoulou et al., 2009).

3. Results and discussion

3.1. Performance evaluation of BUL, UCD and UCM experiments

Fig. 2 presents the diurnal variation of SAT, averaged for July 24–26 2009, from observations and simulations over the 19 THERMO-POLIS2009 campaign ground-based meteorological stations used in the current study at the GAA. The maximum temperature over the majority of the urban sites exceeded 37 °C, while the minimum temperature during the night over the HIR areas, which are located in the city core, remained above 28 °C. A much lower daily maximum temperature was observed over rural territories (NVM at Pikermi; Fig. 2s). These features indicate that the effect of the 3-day heat wave episode is amplified by the UHI in the interior urban fabric of Athens.

The BUL experiment lacks ability in simulating the magnitude of the diurnal variation of SAT, as it significantly underestimates the daily maximum temperature over all urban stations. It is characteristic that the absolute maxima daytime model errors vary from − 1.74 °C (LIR-4 at Papayannis; Fig. 2d) to − 5.2 °C (HIR-6 at Thiseio; Fig. 2m). Thus, it is evident that the BUL simulation cannot capture the high-temperature weather pattern and the SAT temperature contrast between the urban and rural districts. This poor performance arises mainly from the inadequate representation of the urban environment in the BUL scenario. In particular, it seems that the modified land surface properties used by Noah LSM (Section 2.2) to describe the atmospheric and thermal dynamics in cities are deficient for capturing the sub-grid scale features of the UHI effect. The main disadvantage of this approach is that it considers urban surfaces as homogeneous and flat, while urban environments are more complicated in reality, with different artificial and natural surfaces.

UCD and UCM experiments provide a more detailed approach for handling the characteristics of the different urban LULC types and take into account the thermal and radiative processes related to the urban geometry. However, it is interesting to see that the UCD simulation is not capable of producing better results compared to the BUL scenario. Contrary, Fig. 2 illustrates that UCD simulates slightly lower daily temperatures. One important reason for this is the introduction of pervious, grass-covered land into the urban grid cells through the F$_{urb}$ parameter. The role of urban grass is more evident during the night

Table 3
Values of the surface properties and UCPs used in the present study.

Parameter	Albedo, dimensionless (percentage change)			Emissivity, dimensionless (percentage change)			Building height, m (percentage change)			Road width, m (percentage change)			Urban fraction, % (percentage change)		
Scenario	LIR	HIR/UB	IC	LIR	HIR/UB	IC	LIR	HIR/UB	IC	LIR	HIR/UB	IC	LIR	HIR/UB	IC
BUL	0.15	0.15	0.15	0.88	0.88	0.88	-	-	-	-	-	-	-	-	-
UCD	0.15	0.15	0.15	0.88	0.88	0.88	5	7.5	10	8.3	9.4	10	50	90	95
UCM	0.15	0.15	0.15	0.88	0.88	0.88	5	7.5	10	8.3	9.4	10	50	90	95
UCM_SAL	0.09 (−40%)	0.10 (−33.3%)	0.11 (−26.7%)	0.88	0.88	0.88	5	7.5	10	8.3	9.4	10	50	90	95
UCM_SEM	0.15	0.15	0.15	0.97 (+10.2%)	0.97 (+10.2%)	0.97 (+10.2%)	5	7.5	10	8.3	9.4	10	50	90	95
UCM_SBH	0.15	0.15	0.15	0.88	0.88	0.88	2.5 (−50%)	3.75 (−50%)	5 (−50%)	8.3	9.4	10	50	90	95
UCM_SRW	0.15	0.15	0.15	0.88	0.88	0.88	5	7.5	10	4.15 (−50%)	4.7 (−50%)	5 (−50%)	50	90	95
UCM_SUF	0.15	0.15	0.15	0.88	0.88	0.88	5	7.5	10	8.3	9.4	10	25 (−50%)	45 (−50%)	47.5 (−50%)
UCM_OPT	0.09 (−40%)	0.10 (−33.3%)	0.11 (−26.7%)	0.97 (+10.2%)	0.97 (+10.2%)	0.97 (+10.2%)	9 (+80%)	15 (+100%)	6 (−40%)	10 (+20.5%)	12 (+27.2%)	6 (−40%)	80 (+60%)	90	95

over the LIR sites where the UCD experiment simulates much lower nocturnal SATs. This is because 50% of the LIR grid cells are covered by pervious surface ($F_{urb} = 0.50$), which store less heat during the day and has a higher nighttime cooling rate. As mentioned in Section 2.2, F_{urb} is one of the UCPs required to drive the SLUCM. Hence, it is evident that the SAT results are sensitive to key UCPs. Also, it seems that the default values of UCPs are inappropriate for the city of Athens.

The impact of F_{urb} on night time LIR SATs is also present during the UCM simulation, while it is also evident that UCM produces even lower temperatures over the majority of the urban stations during the night, resulting to higher negative biases. On the other hand, the modified SLUCM code used in the UCM scenario reduces remarkably the daytime biases compared to the other two experiments. This performance is primarily attributed to the revised calculation of the impervious surface temperature (Eq. (5)) during the UCM experiment. In particular, Eq. (5) combines the temperatures of roofs and street canyon. The complex canyon geometry increases the urban surface compared to a plane area and introduces radiation-trapping effects. Hence, more radiant energy can be absorbed and trapped, contributing to higher urban surface temperatures during both the day and night (see Supplementary material Figs. S1a, b). Roof temperatures have a different contribution in Eq. (5). Because roofs are more exposed to the open sky, they absorb more shortwave radiation during the day, whereas they emit more longwave radiation in the night. Thus, the temperatures of roofs increase further the daytime impervious surface temperatures, while they decrease the urban surface temperatures significantly following sunset (see Supplementary material Figs. S1c, d). Overall, the UCM scenario reproduces more accurately the diurnal variation of temperatures over the majority of the urbanized sites. The existence of UHI, revealing from the excess warmth of the urban stations in comparison with the rural one, is captured well by the UCM simulation. Additionally, the absolute errors from the measured extreme, due to the heat wave episode, daytime maximum temperatures are limited to a range from − 3.49 °C (LIR-3 at Nea Filadelfia; Fig. 2c) to 1.28 °C (IC-1 at Elefsina; Fig. 2n). Thus, it is pronounced that the estimation of correct urban surface temperatures through Eq. (5) is crucial for simulating air temperatures that are closest to reality.

Even so, the model results still deviate noticeably from the observations. As already pointed out, this is probably caused by the irrelevant for the study area UCPs. Despite the increasing effort in developing UCP data sets by utilizing remote-sensing data and multiple GIS techniques (Ching et al., 2009; Ratti et al., 2002; Burian et al., 2004; Molnár et al., 2016), the availability of such data is limited to a few geographical locations. Thus, it is necessary to analyze the sensitivity of the modeled urban temperatures to critical UCPs and adapt their values for the GAA.

3.2. Sensitivity analysis

To quantify the impact of the selected factors on the spatial distribution of urban temperatures, the partial derivative of SAT on each parameter (xx) was calculated as the fraction of the SAT difference between the corresponding UCM_Sxx experiment and the UCM simulation to the relative xx difference:

$$\frac{\partial \mathrm{SAT}}{\partial \mathrm{xx}} = \frac{\mathrm{SAT}_{\mathrm{UCM.Sxx}} - \mathrm{SAT}_{\mathrm{UCM}}}{\mathrm{xx}_{\mathrm{UCM.Sxx}} - \mathrm{xx}_{\mathrm{UCM}}} \tag{7}$$

The values of SAT on Eq. (1) were averaged for the three-day heat wave period (July 24–26, 2009) and the analysis focused on the daytime (1200 UTC) and nighttime (0200 UTC). Figs. 3–7 presents the spatial distributions of SAT sensitivities to each studied parameter over the urban grid cells as well as the diurnal variation of the averaged SAT from observations and simulations at six characteristic sites.

3.2.1. Surface albedo

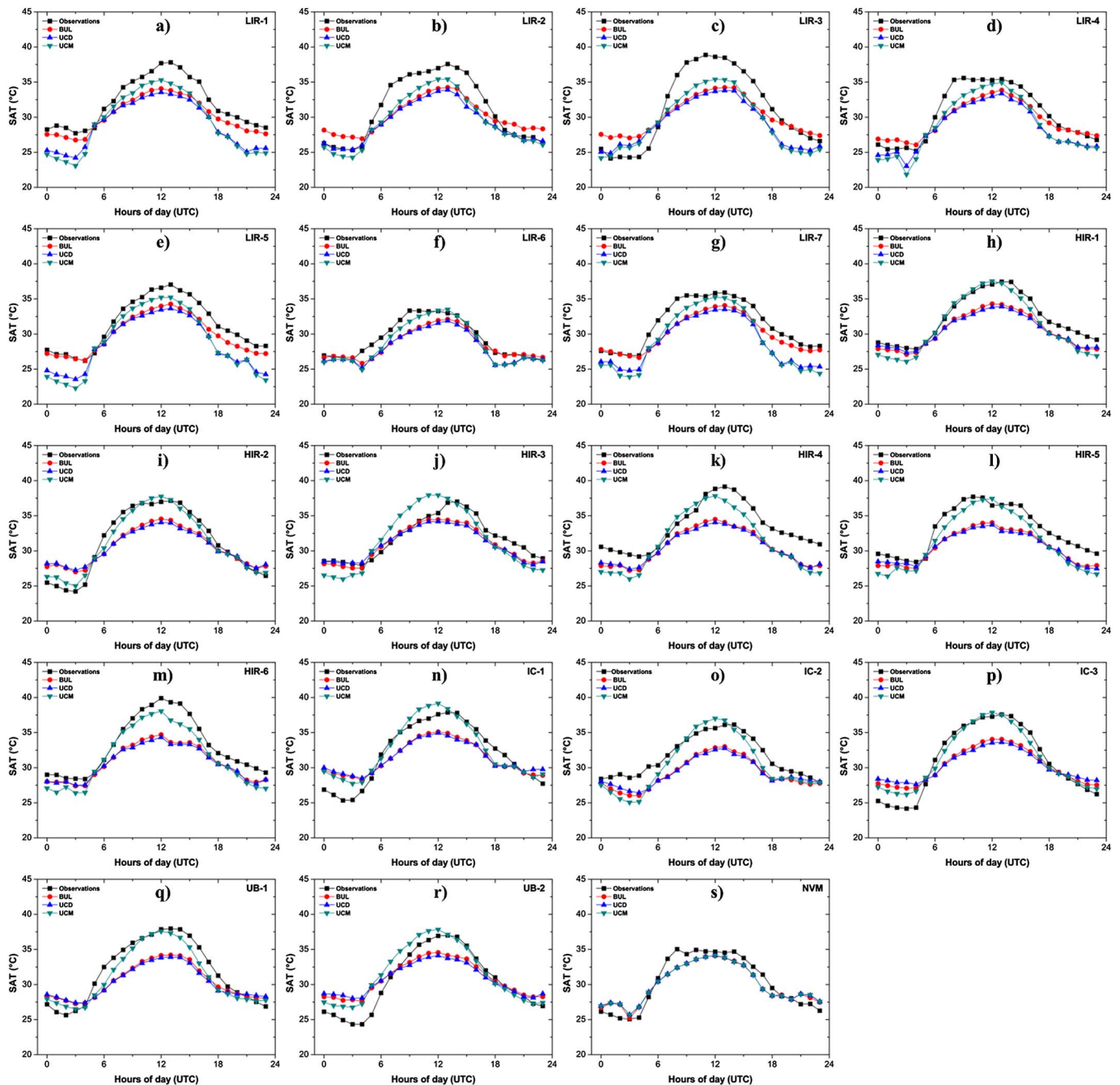Albedo is critical for the radiation balance of any surface, as it

Fig. 2. Diurnal variation in near-surface air temperature from ground-based observations and BUL, UCD, and UCM numerical experiments over LIR (a–g), HIR (h–n), IC (p–r), UB (s–t), and NVM (u) sites. Values are averaged for 24–26 July 2009.

represents the portion of the incoming shortwave solar radiation that is reflected back to the atmosphere. Lower values, as in the UCM_SAL scenario, lead to an increased absorption of radiation and, consequently, to a higher surface net radiation. Due to the negligible irrigation, the reduced moisture availability and the absence of vegetation, small latent heat fluxes are observed in urban areas (Christen and Vogt, 2004). As a result, the surplus of daytime radiant energy is partitioned into sensible heat flux, while the remainder is consumed in increasing the daytime surface heat storage. The daytime upward sensible heat flux warms the overlying air by conduction and advection (Oke, 1987). This leads to higher SAT, as Fig. 3b indicates. The impact of this process is greater over the UB, HIR, and IC regions because of the higher (less) urban fraction (vegetation fraction) that characterizes these sites. It is characteristic that a reduction of albedo by 1 (0.1) over the central

urban fabric of Athens, where the HIR stations are located, results in an increase of the simulated SAT by 7.10 (0.71) °C to 8.33 (0.83) °C.

The UCM_SAL experiment also simulated higher values of air temperature over the majority of the urban grid cells during the night, as Fig. 3a illustrates. This is caused by the release of the enhanced daytime heat storage that begins during the evening transition and hinders the nocturnal fall of the SAT. The complex canyon geometry contributes further to this direction, as it inhibits the efficiency with which the urban areas lose heat through radiative cooling. However, there are some regions (e.g. LIR-1 at Ilioupoli) where the modeled SAT was decreased, with the reduction reaching up to 10.60 (1.06) °C per 1 (0.1) unit of albedo decrease. These outliers are associated with albedo-induced changes on the local atmospheric circulation. In particular, the wind speed was reduced over the exceptionally urban grid cells, leading
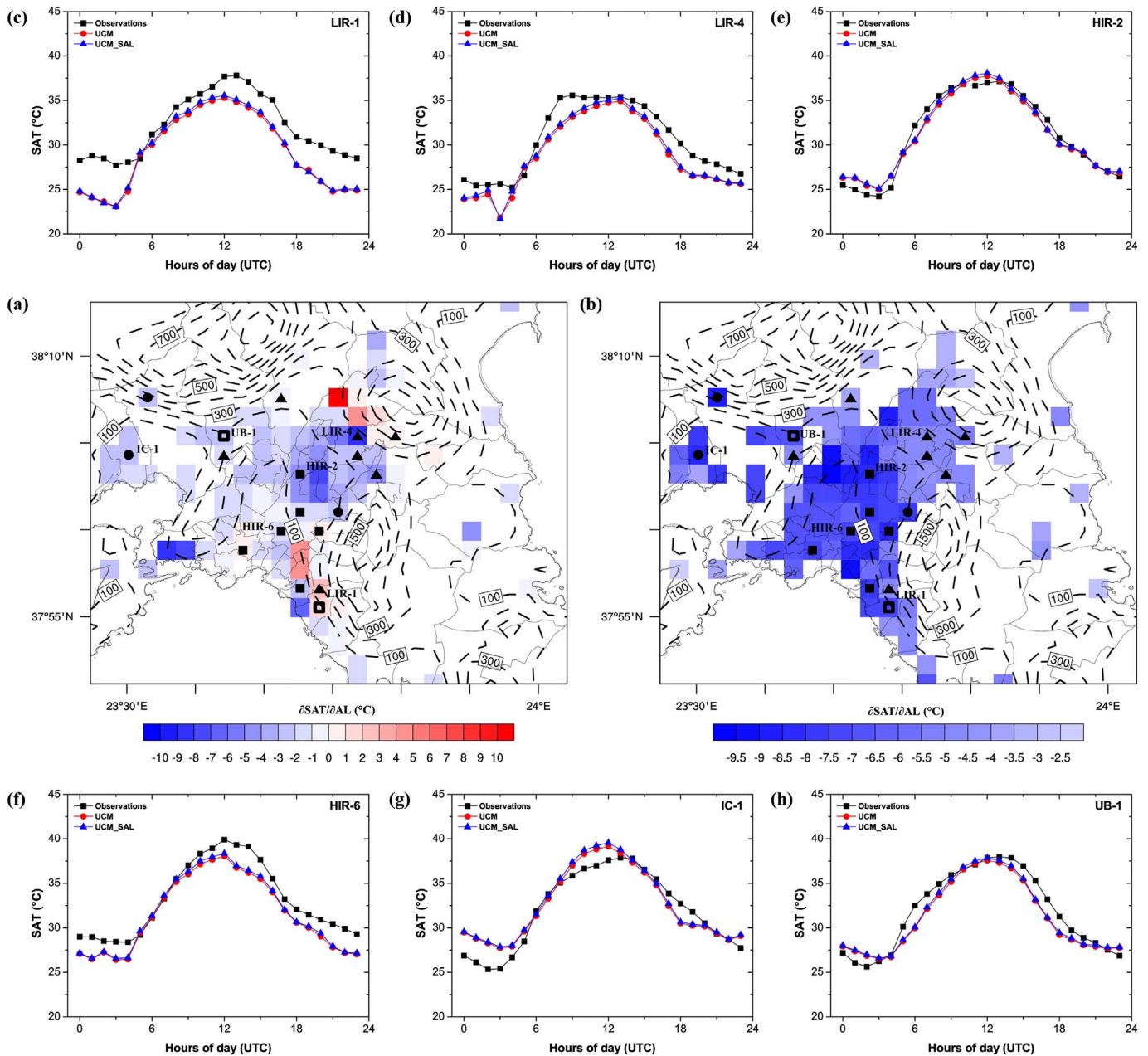
Fig. 3. Spatial distribution of SAT sensitivities to surface albedo during (a) the night, and (b) the day. (c–h) Diurnal variation in SAT from ground-based observations and UCM, and UCM_SAL numerical experiments over six characteristic sites. Values are averaged for 24–26 July 2009.

to a decrease of the nighttime downward sensible heat flux of both pervious and impervious surface. As a result, the vegetated LST, calculated by the Noah LSM, was reduced. Thus, the total grid LST was decreased as well as the SAT, consequently. It is worth mentioning that the impervious LST was not affected by the reduction of the urban sensible heat flux because of its modified calculation in the SLUCM code (Eq. (5)). The aforementioned analysis is included in the Supplementary material (Figs. S2–S8) and shows that the spatiotemporal variability of urban temperatures is not only dependent on the land surface and urban geometry characteristics, but also on the local meteorological circulations.

In more detail, the modification of wind circulation could be attributed to the change of the thermal structure of the atmosphere at a local scale due to the modification of albedo in the urban areas. This is because the wind speed is driven by pressure gradient forces depending on horizontal temperature gradients and altitude variations (Kumar et al., 2014). Particularly for the night, Fig. S2a (see Supplementary

material) illustrates that the mean synoptic flow modeled by the UCM simulation is north-northwest. Wind speeds are higher than 10 m/s in the complex terrain areas close to mountains Parnitha and Penteli, whereas the wind is much lower in the urban fabric of Athens. During the UCM_SAL experiment (see Supplementary material Fig. S2b), even though the circulation pattern is the same, a modest displacement of the sea level pressure gradients is evident. Hence, the indirect interaction between the albedo change and local atmospheric dynamics influences the urban temperatures and contributes to the UCM_SAL model response.

3.2.2. Surface emissivity

The role of surface emissivity in UHI causation is frequently ignored, as noted by Oke et al. (1991). However, a surface with increased emissivity remains cooler because it emits more longwave radiation to the open space. Consequently, less heat is transmitted to the atmosphere leading to lower air temperatures.
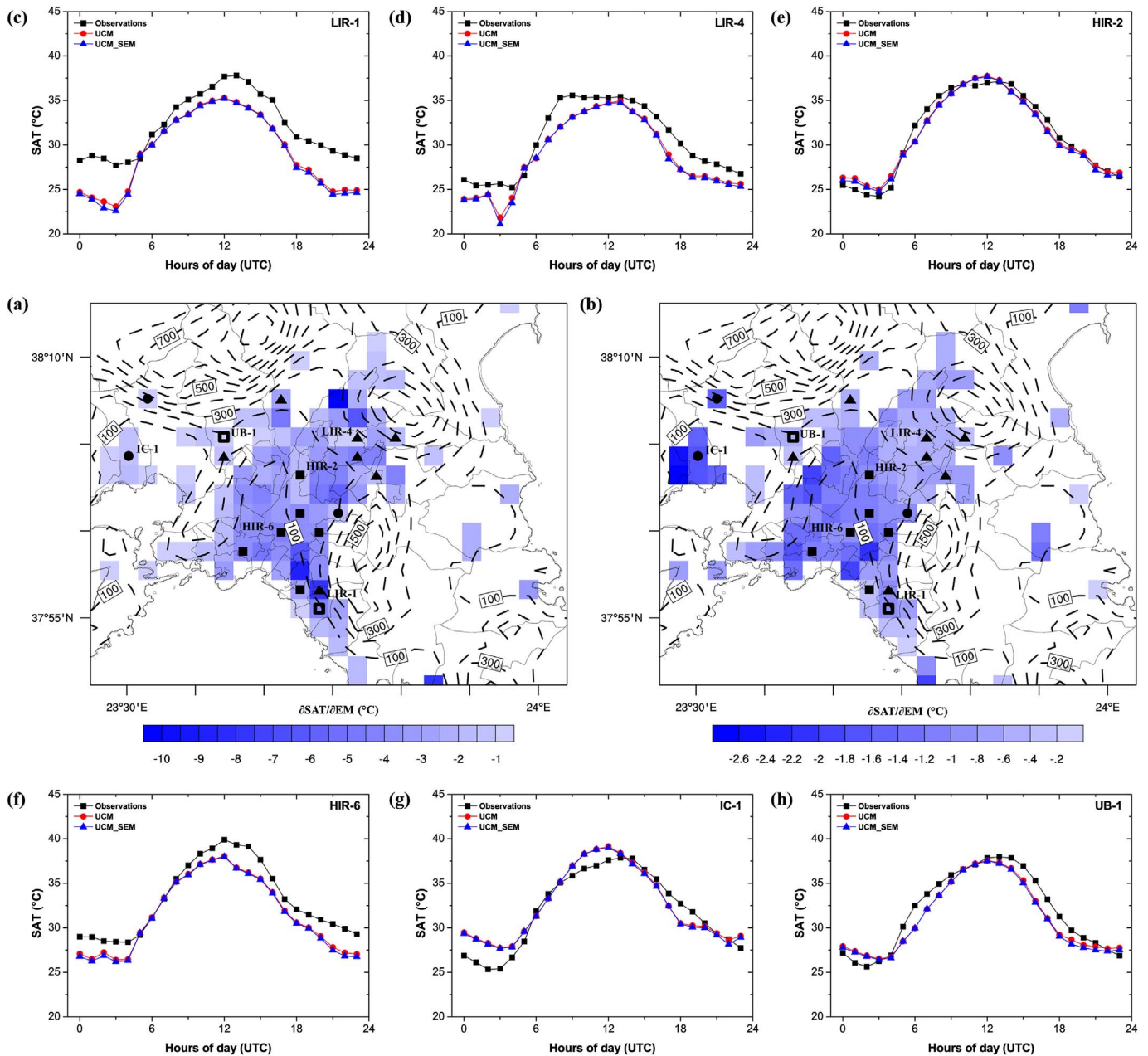
Fig. 4. Spatial distribution of SAT sensitivities to surface emissivity during (a) the night, and (b) the day. (c–h) Diurnal variation in SAT from ground-based observations and UCM, and UCM_SEM numerical experiments over six characteristic sites. Values are averaged for 24–26 July 2009.

Indeed, Fig. 4 shows that the model simulates a reduction of SAT when the emissivity of the urban surface and facets was raised from 0.88 to 0.97. As solar shortwave radiation reduces to zero during the night, the main driver of the surface energy balance is the outgoing longwave terrestrial radiation. As a result, the sensitivities of the SAT to emissivity are higher during the nighttime (Fig. 4a), varying, on average, from − 1.33 (0.13) °C per 1 (0.1) unit of change over IC sites to − 2.84 (or 0.28) °C/1(0.1) emissivity change over LIR stations, and to − 3 (0.3) °C/1(0.1) emissivity change over HIR and UB areas. It is worth mentioning that these values are comparable to those found in the studies of Atkinson (2003) and Hamdi and Schayes (2008). However, over two regions located at the foot of mountain Penteli and Hymettus, respectively, the reduction of the simulated SAT reach up to 10.70 (1.07) °C per 1 (0.1) unit of emissivity increase. These exceptional sensitivities are originated from the alteration of local wind circulation as in the case of the albedo-induced outliers reported in Section 3.2.1. Fig. S2c (see Supplementary material) shows that the shift of the

local atmospheric pressure systems during UCM_SEM experiment is even higher than in the UCM_SAL (see Supplementary material Fig. S2b) scenario, indicating stronger variations in the wind. The fact that the exceptional diversities in the simulated temperatures response are located in the same territories as those during the UCM_SAL experiment shows that the complicated geomorphology of the study area plays an important role by introducing local heterogeneities and dynamical effects, especially during the night when the mechanical turbulence is dominant.

During the day, the outgoing thermal radiation flux has a less important role in regulating the radiation balance. Thus, the increase of emissivity leads to lower modeled SAT reduction (Fig. 3b). The urban air temperature decrease per 1 (0.1) unit of emissivity increase varies, on average, from 0.5 (0.05) °C at suburban areas (LIR) to 0.82 (0.08) °C over the HIR and UB sites, and to 1.4 (0.14) °C over industrial and commercial (IC) areas. These daytime variations, as well as those above during the night, arise from the different street canyon morphology and
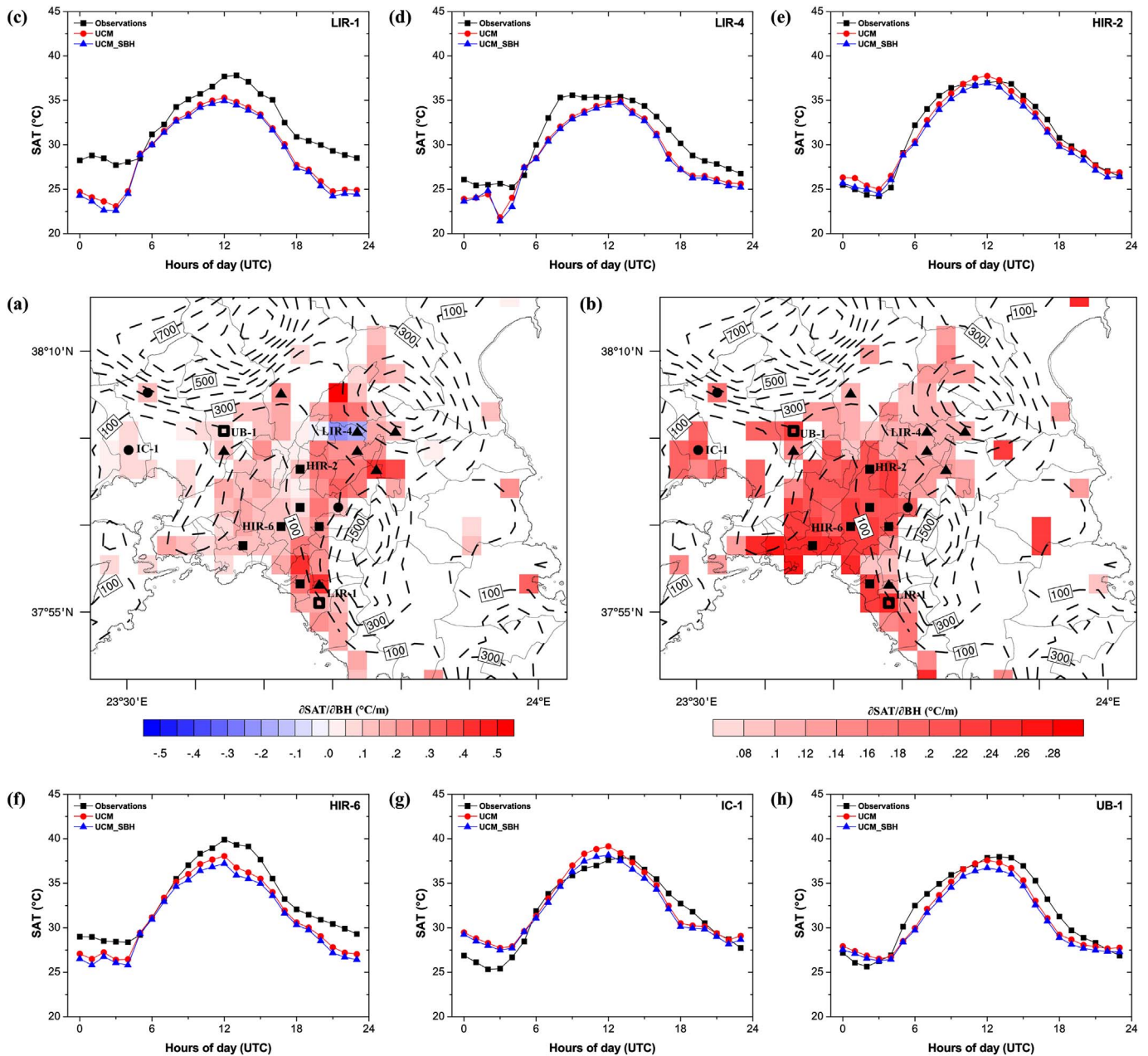
Fig. 5. Spatial distribution of SAT sensitivities to mean building height during (a) the night, and (b) the day. (c–h) Diurnal variation in SAT from ground-based observations and UCM, and UCM_SBH numerical experiments over six characteristic sites. Values are averaged for 24–26 July 2009.

topography of each urban LUCL type, resulting in various radiative geometry (e.g. radiation trapping) effects.

3.2.3. Mean building height

The mean height of buildings is involved in the parameterization of three important physical processes in the urban boundary layer (UBL), simulated by the SLUCM. Firstly, building heights control the shadow effects in the street canyons (Kusaka et al., 2001). The second parameterization influenced by the building heights is the sky view factor (SVF) (Oke, 1988), i.e. the portion of the earth's atmosphere that can been seen from a given point on the street canyon, which has a significant effect on the efficiency with which the urban canyons can lose heat through the escape of outgoing long-wave radiation to the open sky. Last, but not least, the mean building height (BH) affects the parameterization of the roughness length parameters mentioned in Section 2.2, and, consequently, impacts the turbulent mixing processes and urban canopy wind speed.

Having the above in mind, lower BHs, as in the UCM_SBH experiment, lead to lower shading and as a result, the urban surface tends to warm and to store more heat during the day. Thus, it would be expected that higher daytime SATs would be modeled. However, Fig. 5b highlights positive $\partial SAT/\partial BH$ sensitivities, indicating that the reduction of BH resulted in lowering urban temperatures. This is because the UCM_SBH simulated lower urban roughness length parameters and greater values of SVF, compared to UCM scenario (see Supplementary material Table S2). During the day, smaller thermal roughness ($z0_t$) values reduce the turbulent heat exchange (Voogt and Grimmond, 1999) through the UBL and results to lower air temperatures. Additionally, the reduction of the urban aerodynamic roughness length factors, i.e. $z0_c$ and $z0_r$, led to less drag and blocking effects. As a result, the UCM_SBH wind velocities in the urban canopy were stimulated and, in turn, the near-surface air cooling was enhanced. Higher values of SVF also contributed to heat loss, even though the radiative cooling has a secondary role after the sunrise. The SAT reduction is larger over HIR,
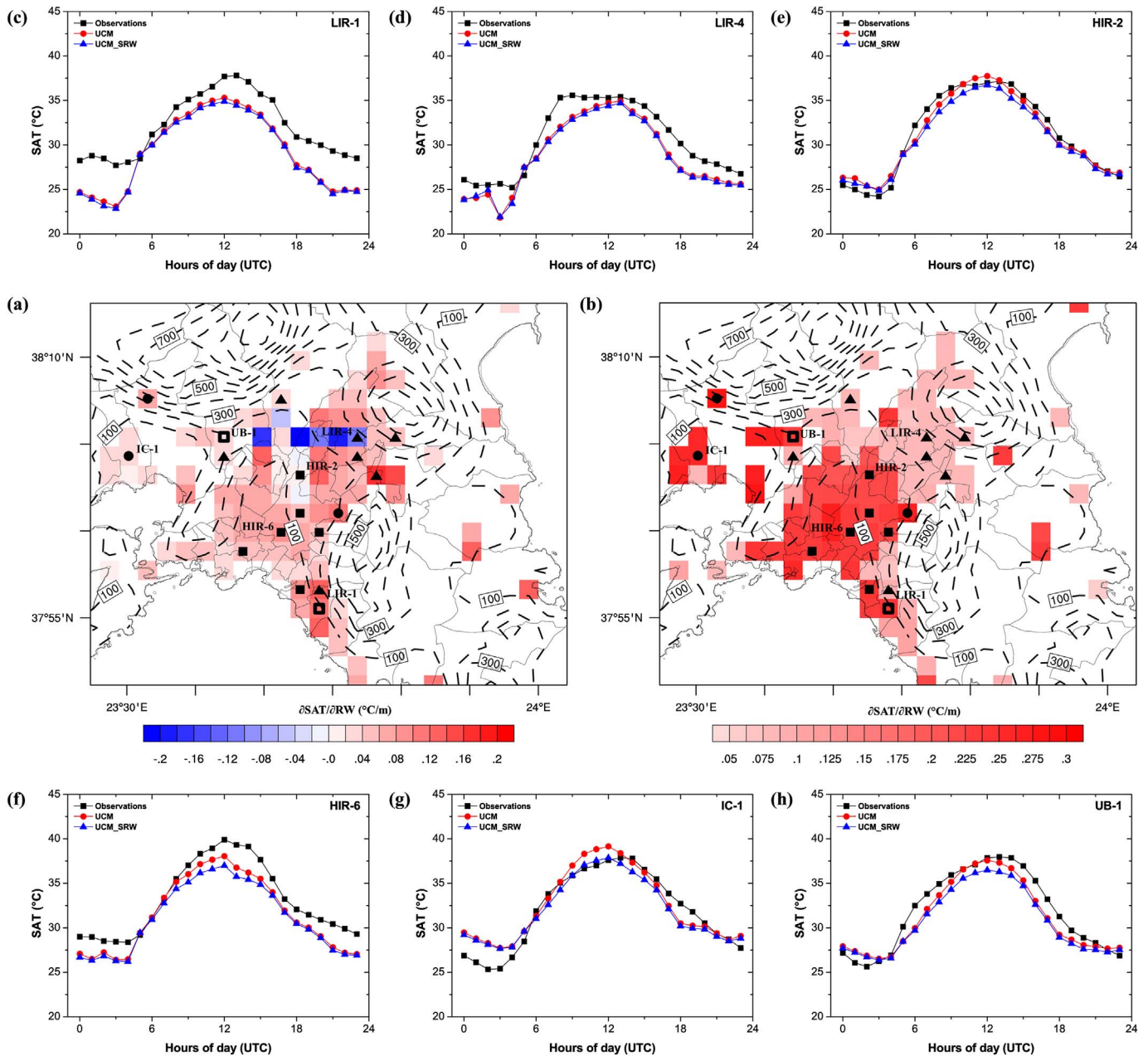
Fig. 6. Spatial distribution of SAT sensitivities to road width during (a) the night, and (b) the day. (c–h) Diurnal variation in SAT from ground-based observations and UCM, and UCM_SRW numerical experiments over six characteristic sites. Values are averaged for 24–26 July 2009.

UB, and IC areas, reaching up to 0.27 °C/m, due to the higher urban fraction that characterizes these LULC categories.

In the nighttime, shear plays the dominant role in the development of mechanical turbulence (Cao and Lin, 2014), which is responsible for the downward entrainment of hot air at the elevated inversion base. The decreased $z0_c$ and $z0_r$ values during the UCM_SBH scenario weakened the production of shear and resulted in the simulation of lessened SATs over the majority of the urban grid cells, as Fig. 5a illustrates. The enhanced SVF values contributed further to this direction because of the more efficient post-sunset radiative cooling. The sensitivities of nocturnal SAT to BH ranges from 0.05 °C/m to 0.25 °C/m over the HIR, UB, and IC sites, while they take their higher values (up to 0.55 °C/m) in the suburban areas.

On the other hand, the modeled SAT was increased by 0.16 °C/m (LIR-4 at Papayannis) and 0.22 °C/m over two suburb areas, located close to mountain Penteli. Fig. S2d (see Supplementary material) highlights that these areas are exposed to steep wind speeds due to the

complex topography of the region, while an alteration of the mean sea level pressure gradient is evident compared with the UCM simulation (see Supplementary material Fig. S2a). Thus, these abnormal sensitivities are the result of the same local dynamical effect as that which produced the outliers during the UCM_SAL and UCM_SEM simulations. This time the change in the local circulation acted on the opposite direction. The wind speed was increased, and therefore the downward sensible heat flux was strengthened, especially over the previous surface. Hence, the LST$_{veg}$ was increased and led to the rise of the total grid LST and, consequently, of the SAT (see Supplementary material Figs. S9–S15).

3.2.4. Road width

The road width (RW) parameter in SLUCM affects the same physical processes as those mentioned in Section 3.2.3 for BH. Also, it influences the computation of the revised impervious surface temperature (Eq. (5)) by moderating the weighted factor F_{roof} (Eq. (6)). In particular, the
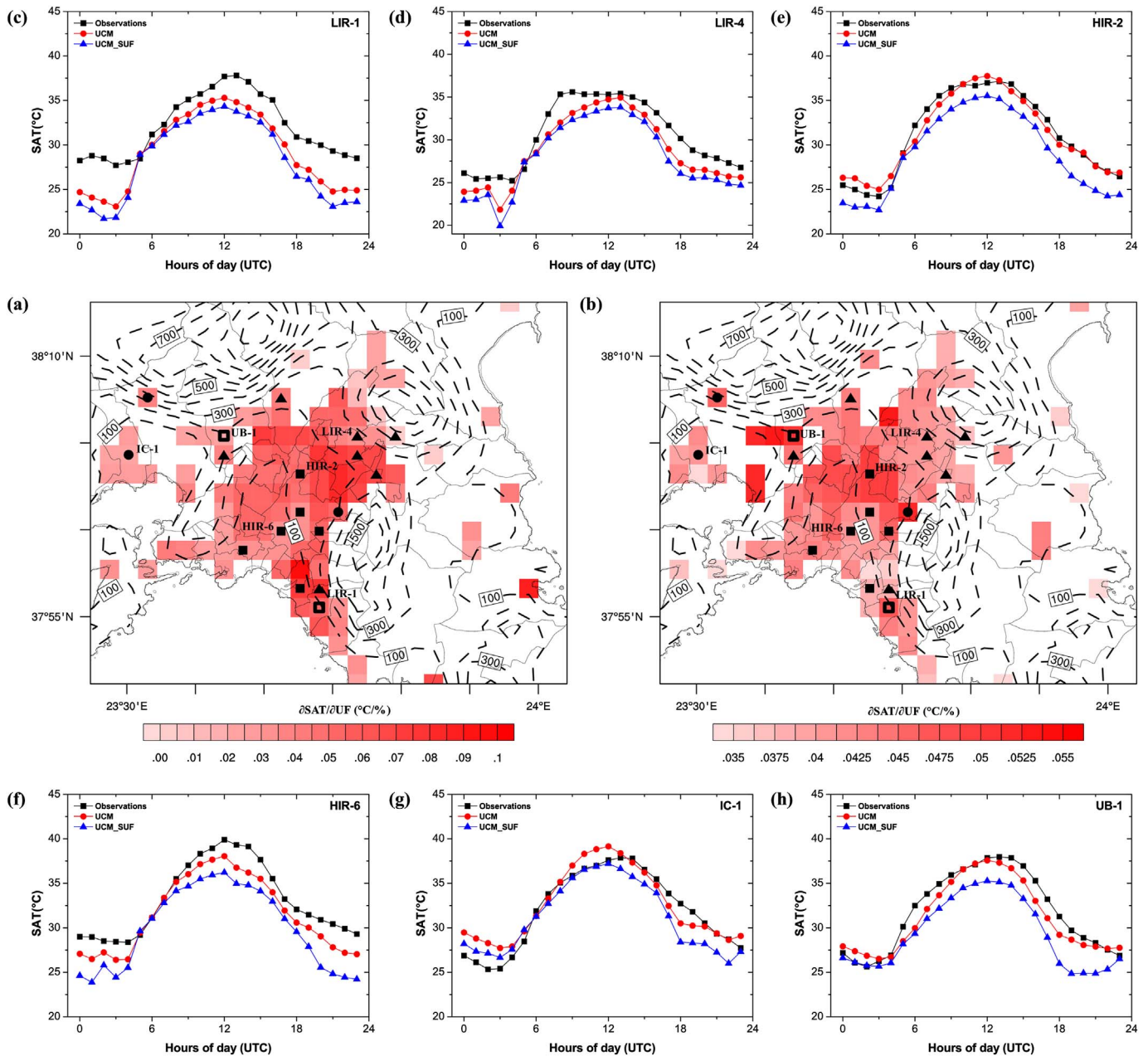
Fig. 7. Spatial distribution of SAT sensitivities to urban fraction during (a) the night, and (b) the day. (c–h) Diurnal variation in SAT from ground-based observations and UCM, and UCM_SUF numerical experiments over six characteristic sites. Values are averaged for 24–26 July 2009.

reduction of RW in the UCM_SRW simulation led to (a) more shading, (b) reduced thermal and aerodynamic roughness length parameters, (c) lower SVF values, (d) decreased urban canopy wind speeds, and (e) larger F_{roof}, in comparison with UCM scenario (Supplementary material Table S2).

Enhanced shadowing during the day, results in less available heat in the street canyons. Moreover, as in the UCM_SBH experiment, the turbulent heat transfer is weakened due to the lower $z0_t$ values, while the decreased $z0_c$ and $z0_r$ would expected to lead to higher canopy winds. However, the canopy wind is lower during UCM_SRW simulation because narrow street canyons do not favor the development of steep wind speeds. Additionally, the reduced SVFs introduce less longwave radiation loss. While roof surfaces are warmer than the street canyons during the day because they are more exposed to solar radiation and, consequently, absorb more short-wave radiant energy (see Supplementary material Fig. S1a, c). The greater F_{roof} increased the contribution of T_{roof} in the modified calculation of the LST_{urb} (Eq. (5)),

and, taking into account that the SLUCM simulates higher values of T_{roof} compared to the T_{canyon} values, this led to the rise of the impervious surface temperatures. The last modifications counteract the first two, concerning the evolution of urban air temperatures. However, as Fig. 6b indicates, the higher shadow effects and the lower heat turbulence are dominating and lead to the simulation of lessened daytime SATs. The spatial distribution, as well as the magnitude, of SAT reduction during the day is the same as in the UCM_SBH simulation. The higher sensitivities to RW appearing over the sites with the larger urban fraction, ranging, on average, from 0.23 °C/m over the HIR and UB sites to 0.27 °C/m over the IC stations.

During the night, despite the reduced radiative cooling in the street canyons due to the decreased SVF, the UCM_SRW experiment also simulated lower urban temperatures over the most of the urban LULC cells (Fig. 6a). This is because the roofs cool more efficiently than the urban canyon (see Supplementary material Figs. S1b,d) and, hence, the larger roof fraction led to decreased simulated LST_{urb} values.

Furthermore, as in the UCM_SBH simulation, the decreased urban aerodynamic roughness lengths resulted in significantly inhibited mechanical turbulence, reducing the entrainment of hot air from the free troposphere in the UBL. As Fig. 6a highlights, the magnitude of the SAT decrease is greater over the LIR locations, reaching up to 0.20 °C per 1 m of RW.

The unexpected increase of nocturnal SATs over some regions, positioned between, and at the foot of, mountain Penteli and Parnitha, is attributed to the alteration of the local wind pattern (see Supplementary material Fig. S2e), as it was described in Section 3.2.3 for the BH-induced outliers. Also, it is worth mentioning that the change of RWs and BHs can affect the anthropogenic heat released in the urban areas. However, as denoted in Section 2.3.2, no AH was considered in the model set-up because of the lack of a relevant inventory for the city of Athens. Therefore, it is important to emphathize that changes in the AH do not affect the UCM_SBH and UCM_SRW simulations, and, consequently, the results discussed above.

3.2.5. Urban fraction

As noted in previous sections, the urban fraction variable has a critical role in the coupling of WRF/Noah modeling system with the SLUCM and affects the simulated urban temperatures directly, especially during the night. Fig. 7 highlights this influence of F_{urb} on the modeled thermal environment of Athens. The reduction of F_{urb} by 50% during the UCM_SUF experiment leads to a reduction of, both daytime and nighttime, SATs. The sensitivities of SAT spans from 0.030 °C/% to 0.055 °C/% during the day, while they take higher values that reach up to 0.1 °C/% during the night.

This is because the greater portion of urban vegetation modifies the SEB compared to the UCM simulation. The increased grass-covered land on the sub-grid scale introduces larger amounts of moisture availability and, consequently, shifts the partitioning of the energy budget from sensible to latent heat flux. As a result, the evaporative cooling of the total grid surface is enhanced, and the urban temperatures drop during the day (Fig. 7b). Additionally, the vegetation thermal properties account for the lower daytime total-grid heat storage and the higher nighttime cooling rate that lead to a greater reduction of nocturnal SATs (Fig. 7a). The results above are in agreement with those of other studies investigated the potential beneficial effects of decreasing (increasing) the urban (vegetation) fraction in cities (Shashua-Bar and Hoffman, 2000; Hamdi and Schayes, 2008; Papangelis et al., 2012).

3.3. Validation of UCM_OPT

Three statistical metrics, namely: (i) the mean bias error (MBE), (ii) the mean absolute error (MAE), and (iii) the index of agreement (IOA), were computed for SAT in order to quantitatively compare the model performance between the base case scenario simulation, UCM, and the UCM_OPT simulation with the optimal set of surface and urban canopy parameters. Table 4 shows the calculated model performance measures grouped by the three LULC urban categories, while Fig. 8 presents the spatial distribution of temperature MBs for the two numerical experiments, as well as the diurnal variations of the averaged SAT from observations and simulations at six characteristic measurement stations.

The UCM case produced the largest biases and absolute errors (Table 4). The model was found to highly underestimate the urban

temperatures by − 1.97 °C over the LIR sites, while it overestimated SAT of industrial and commercial regions (IC), as it is evident in Fig. 8a. The calibration of surface properties and UCPs during the UCM_OPT simulation minimized remarkably the errors. In particular, the model was found to be biased cold over the LIR locations, underestimating SAT by 0.39 °C (1.87 °C) in terms of MB (MAE) under the UCM_OPT scenario. Minimal positive biases were occurred for the same experiment in HIR/UB and IC stations where SAT deviates from observations by 2.17 °C and 2.00 °C, respectively. Also, the UCM_OPT simulation produced higher values of IOA over all urban land use classes, indicating a better correlation between the modeled and observed urban temperatures.

The improved model performance over the LIR regions is primarily due to the 80% increase of urban fraction, because SAT is very sensitive to this parameter, as shown in Section 3.2.5. The rise of building heights and road widths also contributed to the more accurate simulation of urban temperatures. Thus, the realistic parameterization of UCPs is crucial for the replication of the elevated temperatures, caused by the synergy of UHI and HW weather conditions, over urban environments. However, the model still lacks ability in representing the nocturnal SATs adequately (and the UHI effect) over some locations (e.g. LIR-1 at Ilioupoli; Fig. 8c, and HIR-6 at Thisio; Fig. 8f). An important source of this inconsistency is the fact that the canopy parameters may vary significantly over the same urban LULC type and even over the same model grid cell that covers an area of 2 km². Hence, the use of a single set of properties over a 2 km² urban area is not completely realistic, especially for the study area, as the city of Athens is characterized by inconsistent urban planning with irregular positioning of buildings (Salvati et al., 2013). Additionally, the ground-based measurements usually represent the weather conditions over a limited area of 1 km². Thus, the spatial disparity between the observations and the modeled output contributes to the model biases.

4. Conclusions

In the current study, a mesoscale NWP model (WRF) was used for investigating the spatial and temporal distribution of near-surface air temperature at an urban scale. Urban temperatures are directly affected by the UHI effect, and they are amplified during heat wave episodes. For this, the comprehensive modeling study of the present paper was conducted during a 3-day HW event (July 24 to July 26, 2009) over the city of Athens. Observational data obtained during the THERMOPOLIS2009 campaign were used for the same period to evaluate the performance of WRF during various sensitivity scenarios and tune-up its efficiency, concluding to an optimal model configuration that best replicated the temperature distributions.

A set of three numerical sensitivity simulations was carried out to see how the model responds under different urban parameterizations and code modifications regarding temperature changes over time and space. The use of the revised calculation of the impervious surface temperature in the WRF/SLUCM modeling system (Li and Bou-Zeid, 2014) reproduced more accurately the observed diurnal variation of urban temperatures, compared to the bulk and the default SLUCM configurations, and captured the existence of Athens' heat island satisfactorily. The largest improvements were found for the daytime maximum temperatures, while the nocturnal temperature biases were

Table 4
SAT statistical measures for UCM and UCM_OPT experiments.

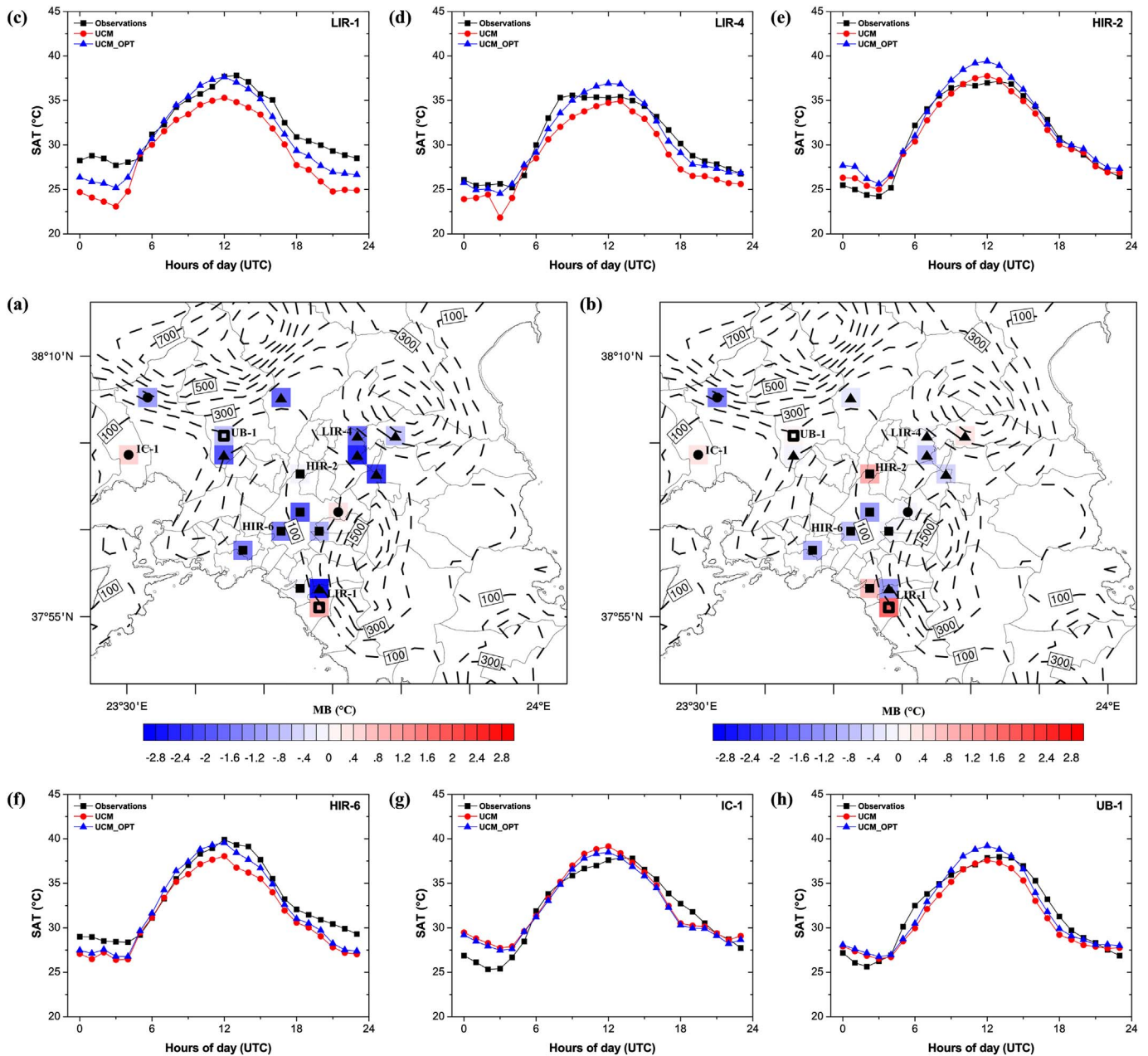| Scenario	MB			MAE			IOA		
	LIR	HIR/UB	IC	LIR	HIR/UB	IC	LIR	HIR/UB	IC
UCM	− 1.97	− 0.76	0.39	2.61	2.18	2.15	0.88	0.90	0.92
UCM_OPT	− 0.39	0.06	0.09	1.87	2.17	2.00	0.93	0.91	0.93

Fig. 8. Spatial distribution of SAT mean biases for (a) UCM, and (b) UCM_OPT simulation. (c–h) Diurnal variation in SAT from ground-based observations and UCM, and UCM_OPT numerical experiments over six characteristic sites. Values are averaged for 24–26 July 2009.

still significant. The latter deviations are of great importance as the UHI effect is primarily a nighttime phenomenon. For this, a series of five additional numerical experiments were implemented to further investigate the sensitivity of the simulated temperatures to highly uncertain land surface and urban canopy properties. The direct sensitivity of urban temperatures to each parameter provided an unprecedented insight on how each parameter affects the UHI causation and evolution:

- The reduction of surface albedo leads to significant increase of daytime temperatures, with maximum sensitivities of around 10 °C (1 °C) per 1 (0.1) unit of albedo change in the calculated range. The same effect, but with a lower magnitude, is produced during the night.
- Surface emissivity has a lower impact on the urban temperatures. The increase of this parameter leads to a maximum temperature decrease of 3 °C (0.3 °C) per 1 (0.1) unit of emissivity change in the range of 0.88 to 0.97 during the night, while the same effect is

imperceptible in the daytime.

- The reduction of mean building height and road width influences various physical processes and mechanisms. In both cases, the mechanisms that contribute to the reduction of urban temperatures dominate during the day, as well as during the night, leading to maximum sensitivities of 0.55 °C/m and 0.27 °C/m for building height and road width, respectively, restricted to the examined values ranges.
- The simulated urban temperatures are highly sensitive to urban fraction. The reduction (increase) of the urban (vegetation) fraction by 1% can lead to a drop in near-surface air temperature by 0.1 °C in the examined range during the night when UHI is more intense. This finding is of great importance as the introduction of green areas (e.g. parks) in Athens could be a very effective mitigation strategy to counteract the UHI effect.

It should be noted that during albedo, emissivity, building height,

and road width sensitivity experiments a few outliers were found in the nighttime over some regions with complex topography. The analysis pointed out that these exceptional sensitivities, showing a different impact on urban temperatures, are associated with induced alterations of the local wind circulation. This reveals that, apart from the surface and street geometry characteristics of a city, the local meteorological conditions affect the intra-urban temperature variability essentially, especially over areas with complex geomorphology and during the night, when the mechanical turbulence is dominant. Anthropogenic heating is also an important factor contributing to the temperature variability in urban areas. However, AH does not affect the results and conclusions mentioned above, as it was not included in the model set-up due to the lack of relevant data. As efforts for the construction of AH emission inventories are increasing, a subsequent study focusing on the sensitivity of the model results to AH could be expected, once such a database exists.

The above findings were used for optimal parameter estimation to enhance the performance of the WRF/SLUCM modeling system over the study area. The optimal model set-up simulation reproduced the observed near-surface air temperature field over the city of Athens, showing lower values of MB ($-0.39\,°C < MB < 0.09\,°C$) and MAE ($1.87\,°C < MAE < 2.17\,°C$), especially over the low-density residential locations. The improved performance in matching the observed urban temperatures is attributed to the use of more accurate land surface and urban canopy properties, which are consistent with the actual city surface and geometry characteristics. This gives confidence that the model is robust and, although further improvements in certain areas of steep topography and in AH effects need to be carried out, can be used for studying the UHI effect and its role in heat-related health effects in the GAA in the projected warmer future climate.

Supplementary data to this article can be found online at https://doi.org/10.1016/j.atmosres.2017.10.015.

Acknowledgements

References

Arnfield, A.J., 2003. Two decades of urban climate research: a review of turbulence, exchanges of energy and water, and the urban heat island. Int. J. Climatol. 23, 1–26. http://dx.doi.org/10.1002/joc.859.

Atkinson, B.W., 2003. Numerical modelling of urban heat-island intensity. Boundary-Layer Meteorol. 109, 285–310. http://dx.doi.org/10.1023/A:1025820326672.

Ban-Weiss, G.A., Woods, J., Levinson, R., 2015a. Using remote sensing to quantify albedo of roofs in seven California cities, part 1: methods. Sol. Energy 115, 777–790. http://dx.doi.org/10.1016/j.solener.2014.10.022.

Ban-Weiss, G.A., Woods, J., Levinson, R., 2015b. Using remote sensing to quantify albedo of roofs in seven California cities, part 2: results and application to climate modeling. Sol. Energy 115, 791–805. http://dx.doi.org/10.1016/j.solener.2014.10.041.

Beniston, M., 2004. The 2003 heat wave in Europe: a shape of things to come? An analysis based on Swiss climatological data and model simulations. Geophys. Res. Lett. 31. http://dx.doi.org/10.1029/2003GL018857.

Best, M.J., 2005. Representing urban areas within operational numerical weather prediction models. Bound.-Layer Meteorol. 114, 91–109. http://dx.doi.org/10.1007/s10546-004-4834-5.

Burian, S., Stetson, S.W., Han, W., Ching, J.S., Byun, D.W., 2004. High-Resolution Dataset Of Urban Canopy Parameters For Houston, Texas. Presented at 5th Symposium on the Urban Environment, Vancouver, BC, Canada, August 23–27, 2004.

Cao, M., Lin, Z., 2014. Impact of urban surface roughness length parameterization scheme on urban atmospheric environment simulation. J. Appl. Math. 2014 (2014) Article ID 267683, 14 pages. https://doi.org/10.1155/2014/267683.

Chen, F., Kusaka, H., Bornstein, R., Ching, J., Grimmond, C.S.B., Grossman-Clarke, S., Loridan, T., Manning, K.W., Martilli, A., Miao, S., Sailor, D., Salamanca, F.P., Taha, H., Tewari, M., Wang, X., Wyszogrodzki, A.A., Zhang, C., 2011. The integrated WRF/urban modelling system: development, evaluation, and applications to urban environmental problems. Int. J. Climatol. 31, 273–288. http://dx.doi.org/10.1002/joc.

2158.

Chen, F., Yang, X., Zhu, W., 2014. WRF simulations of urban heat island under hot-weather synoptic conditions: the case study of Hangzhou City, China. Atmos. Res. 138, 364–377. http://dx.doi.org/10.1016/j.atmosres.2013.12.005.

Ching, J., Brown, M., Burian, S., Chen, F., Cionco, R., Hanna, A., Hultgren, T., McPherson, T., Sailor, D., Taha, H., Williams, D., 2009. National urban database and access portal tool. Bull. Am. Meteorol. Soc. 90, 1157–1168. http://dx.doi.org/10.1175/2009BAMS2675.1.

Christen, A., Vogt, R., 2004. Energy and radiation balance of a central European City. Int. J. Climatol. 24, 1395–1421. http://dx.doi.org/10.1002/joc.1074.

Conti, S., Meli, P., Minelli, G., Solimini, R., Toccaceli, V., Vichi, M., Beltrano, C., Perini, L., 2005. Epidemiologic study of mortality during the summer 2003 heat wave in Italy. Environ. Res. 98, 390–399. http://dx.doi.org/10.1016/j.envres.2004.10.009.

Daglis, I.A., Keramitsoglou, I., Amiridis, V., Petropoulos, G., Melas, D., Giannaros, T., Kourtidis, K., Sobrino, J.A., Manunta, P., Gröbner, J., Paganini, M., Bianchi, R., 2010a. In: Argyriou, A.A., Kazantzidis, A.J. (Eds.), Investigating the Urban Heat Island (UHI) Effect in Athens Through a Combination of Space, Airborne and Ground-based Observations. Proceedings of COMECAP10 (Conference on Meteorology, Climatology and Atmospheric Physics 2010). University of Patras.

Daglis, I.A., Rapsomanikis, S., Kourtidis, K., Melas, D., Papayannis, A., Keramitsoglou, I., Giannaros, T., Amiridis, V., Petropoulos, G., Georgoulias, A., Sobrino, J.A., Manunta, P., Gröbner, J., Paganini, M., Bianchi, R., 2010b. Results of the DUE THERMOPOLIS campaign with regards to the urban heat island (UHI) effect in Athens. In: Proceedings of the ESA Living Planet Symposium 2010, ESA SP-686. European Space Agency.

Dudhia, J., 1989. Numerical study of convection observed during the winter monsoon experiment using a mesoscale two-dimensional model. J. Atmos. Sci. http://dx.doi.org/10.1175/1520-0469(1989)046<3077:NSOCOD>2.0.CO;2.

Dupont, S., Otte, T.L., Ching, J.K.S., 2004. Simulation of Meteorological Fields Within and Above. pp. 111–158.

Founda, D., Giannakopoulos, C., 2009. The exceptionally hot summer of 2007 in Athens, Greece — a typical summer in the future climate? Glob. Planet. Chang. 67, 227–236. http://dx.doi.org/10.1016/j.gloplacha.2009.03.013.

Founda, D., Papadopoulos, K.H., Petrakis, M., Giannakopoulos, C., Good, P., 2004. Analysis of mean, maximum, and minimum temperature in Athens from 1897 to 2001 with emphasis on the last decade: trends, warm events, and cold events. Glob. Planet. Chang. 44, 27–38. http://dx.doi.org/10.1016/j.gloplacha.2004.06.003.

Gabriel, K.M.A., Endlicher, W.R., 2011. Urban and rural mortality rates during heat waves in Berlin and Brandenburg, Germany. Environ. Pollut. 159 (8–9), 2044–2050. http://dx.doi.org/10.1016/j.envpol.2011.01.016.

Georgescu, M., Morefield, P.E., Bierwagen, B.G., Weaver, C.P., 2014. Urban adaptation can roll back warming of emerging megapolitan regions. Proc. Natl. Acad. Sci. U. S. A. 111, 2909–2914. http://dx.doi.org/10.1073/pnas.1322280111.

Giannaros, T.M., Melas, D., Daglis, I.A., Keramitsoglou, I., Kourtidis, K., 2013. Numerical study of the urban heat island over Athens (Greece) with the WRF model. Atmos. Environ. 73, 103–111. http://dx.doi.org/10.1016/j.atmosenv.2013.02.055.

Giannaros, T.M., Melas, D., Daglis, I.A., Keramitsoglou, I., 2014. Development of an operational modeling system for urban heat islands: an application to Athens, Greece. Nat. Hazards Earth Syst. Sci. 14, 347–358. http://dx.doi.org/10.5194/nhess-14-347-2014.

Giannaros, C., Melas, D., Giannaros, T.M., 2017. Evaluation of WRF parameterization schemes during heat-wave events over the greater area of South–East Mediterranean. In: Karacostas, T., Bais, A., Nastos, P. (Eds.), Perspectives on Atmospheric Sciences. Springer Atmospheric Sciences. Springer, Cham.

Hamdi, R., Schayes, G., 2008. Sensitivity study of the urban heat island intensity to urban characteristics. Int. J. Climatol. 28, 973–982. http://dx.doi.org/10.1002/joc.1598.

Heaviside, C., Vardoulakis, S., Cai, X.M., 2016. Attribution of mortality to the urban heat island during heatwaves in the West Midlands, UK. Environ. Health 15. http://dx.doi.org/10.1186/s12940-016-0100-9.

Hong, S., Lim, J., 2006. The WRF single-moment 6-class microphysics scheme (WSM6). J. Korean Meteorol. Soc.

IPCC, 2013. Working Group I Contribution to the IPCC Fifth Assessment Report. Climate Change 2013: The Physical Science Basis. Annex III: Glossary.

Jiménez, P.a., Dudhia, J., González-Rouco, J.F., Navarro, J., Montávez, J.P., García-Bustamante, E., 2012. A revised scheme for the WRF surface layer formulation. Mon. Weather Rev. 140, 898–918. http://dx.doi.org/10.1175/MWR-D-11-00056.1.

Kain, J.S., 2004. The Kain–Fritsch convective parameterization: an update. J. Appl. Meteorol. 43, 170–181. http://dx.doi.org/10.1175/1520-0450(2004)043<0170:TKCPAU>2.0.CO;2.

Kourtidis, K., Georgoulias, A.K., Rapsomanikis, S., Amiridis, V., Keramitsoglou, I., Hooyberghs, H., Maiheu, B., Melas, D., 2015. A study of the hourly variability of the urban heat island effect in the greater Athens area during summer. Sci. Total Environ. 517, 162–177. http://dx.doi.org/10.1016/j.scitotenv.2015.02.062.

Kumar, P., Bhattacharya, B.K., Nigam, R., Kishtawal, C.M., Kal, P.K., 2014. Impact of Kalpana-1 derived land surface albedo on short-range weather forecasting over the Indian subcontinent. J. Geophys. Res. Atmos. 119, 2764–2780. http://dx.doi.org/10.1002/2013JD020534.

Kusaka, H., Kimura, F., 2004. Coupling a single-layer urban canopy model with a simple atmospheric model: impact on urban heat island simulation for an idealized case. J. Meteorol. Soc. Japan 82, 67–80. http://dx.doi.org/10.2151/jmsj.82.67.

Kusaka, H., Kondo, H., Kikegawa, Y., Kimura, F., 2001. A simple single-layer urban canopy model for atmospheric models: comparison with multi-layer and slab models. Boundary-Layer Meteorol. 101, 329–358. http://dx.doi.org/10.1023/A:1019207923078.

Li, D., Bou-Zeid, E., 2013. Synergistic interactions between urban heat islands and heat waves: the impact in cities is larger than the sum of its parts. J. Appl. Meteorol.

Climatol. 52, 2051–2064. http://dx.doi.org/10.1175/JAMC-D-13-02.1.

Li, D., Bou-Zeid, E., 2014. Quality and sensitivity of high-resolution numerical simulation of urban heat islands. Environ. Res. Lett. 9, 55002. http://dx.doi.org/10.1088/1748-9326/9/5/055002.

Liu, Y., Chen, F., Warner, T., Basara, J., 2006. Verification of a mesoscale data-assimilation and forecasting system for the Oklahoma City area during the joint urban 2003 field project. J. Appl. Meteorol. Climatol. 45, 912–929. http://dx.doi.org/10.1175/JAM2383.1.

Loupa, G., Rapsomanikis, S., Trepekli, A., Kourtidis, K., 2016. Energy flux parametrization as an opportunity to get urban heat island insights: the case of Athens, Greece (Thermopolis 2009 campaign). Sci. Total Environ. 542, 136–143. http://dx.doi.org/10.1016/j.scitotenv.2015.10.056.

Macdonald, R.W., Griffiths, R.F., Hall, D.J., 1998. An improved method for the estimation of surface roughness of obstacle arrays. Atmos. Environ. 32, 1857–1864. http://dx.doi.org/10.1016/S1352-2310(97)00403-2.

Martilli, A., 2002. Numerical study of urban impact on boundary layer structure: sensitivity to wind speed, urban morphology, and rural soil moisture. J. Appl. Meteorol. 41, 1247–1266. http://dx.doi.org/10.1175/1520-0450(2002)041<1247:NSOUIO>2.0.CO;2.

Meehl, G.A., Tebaldi, C., 2004. More intense, more frequent, and longer lasting heat waves in the 21st century. Science 305, 994–997. http://dx.doi.org/10.1126/science.1098704.

Meng, W., Zhang, Y., Li, J., Lin, W., Dai, G., Li, H., 2011. Application of WRF/UCM in the simulation of a heat wave event and urban heat island around Guangzhou. J. Trop. Meteorol. 17, 257–267. http://dx.doi.org/10.3969/j.issn.1006-8775.2011.03.007.

Miao, J.F., Chen, D., Borne, K., 2007. Evaluation and comparison of Noah and Pleim-Xiu land surface models in MM5 using GÖTTE2001 data: spatial and temporal variations in near-surface air temperature. J. Appl. Meteorol. Climatol. 46, 1587–1605. http://dx.doi.org/10.1175/JAM2561.1.

Molnár, G., Gyöngyösi, A.Z., Gá, T., 2016. Specification of urban canopy parameters for better understanding the thermal structure in case of Szeged, Hungary. Presented at 16th EMS Annual Meeting & 11th European Conference on Applied Climatology (ECAC), Trieste, Italy, September 12–16, 2016.

Oke, T.R., 1982. The energetic basis of the urban heat island. Q.J.R. Meteorol. Soc. 108, 1–24. http://dx.doi.org/10.1002/qj.49710845502.

Oke, T.R., 1987. Boundary Layer Climates. Methuen and Co., New York.

Oke, T.R., 1988. The urban energy balance. Prog. Phys. Geogr. 12, 471–508. http://dx.doi.org/10.1177/030913338801200401.

Oke, T.R., Johnson, G.T., Steyn, D.G., Watson, I.D., 1991. Simulation of surface urban heat islands under "ideal" conditions at night — part 2: diagnosis of causation. Boundary-Layer Meteorol. 56, 339–358. http://dx.doi.org/10.1007/BF00119211.

Papanastasiou, D.K., Melas, D., Bartzanas, T., Kittas, C., 2010. Temperature, comfort and pollution levels during heat waves and the role of sea breeze. Int. J. Biometeorol. 54, 307–317. http://dx.doi.org/10.1007/s00484-009-0281-9.

Papanastasiou, D.K., Melas, D., Kambezidis, H.D., 2015. Air quality and thermal comfort levels under extreme hot weather. Atmos. Res. 152, 4–13. http://dx.doi.org/10.1016/j.atmosres.2014.06.002.

Papangelis, G., Tombrou, M., Dandou, A., Kontos, T., 2012. An urban "green planning" approach utilizing the weather research and forecasting (WRF) modeling system. A case study of Athens, Greece. Landsc. Urban Plan. 105, 174–183. http://dx.doi.org/10.1016/j.landurbplan.2011.12.014.

Peng, S., Piao, S., Ciais, P., Friedlingstein, P., Ottle, C., Bréon, F.-M., Nan, H., Zhou, L., Myneni, R.B., 2012. Surface urban Heat Island across 419 global big cities. Environ. Sci. Technol. 46, 696–703. http://dx.doi.org/10.1021/es2030438.

Pleim, J.E., 2007. A combined local and nonlocal closure model for the atmospheric boundary layer. Part I: model description and testing. J. Appl. Meteorol. Climatol. 46, 1383–1395. http://dx.doi.org/10.1175/JAM2539.1.

Ratti, C., Di Sabatino, S., Di Sabatino, S., Britter, R., Britter, R., Brown, M., Burian, S., Caton, F., Caton, F., Brown, M., Burian, S., 2002. Analysis of 3-D urban databases with respect to pollution dispersion for a number of European and American cities. Water, Air, Soil Pollut. Focus 2, 459–469. http://dx.doi.org/10.1023/A:1021380611553.

Sailor, D.J., Lu, L., 2004. A top-down methodology for developing diurnal and seasonal anthropogenic heating profiles for urban areas. Atmos. Environ. 38, 2737–2748.

http://dx.doi.org/10.1016/j.atmosenv.2004.01.034.

Sailor, D.J., Georgescu, M., Milne, J.M., Hart, M.A., 2015. Development of a national anthropogenic heating database with an extrapolation for international cities. Atmos. Environ. 118, 7–18. http://dx.doi.org/10.1016/j.atmosenv.2015.07.016.

Salamanca, F., Martilli, A., Yagüe, C., 2012. A numerical study of the urban Heat Island over Madrid during the DESIREX (2008) campaign with WRF and an evaluation of simple mitigation strategies. Int. J. Climatol. 32, 2372–2386. http://dx.doi.org/10.1002/joc.3398.

Salvati, L., Zitti, M., Sateriano, A., 2013. Changes in city vertical profile as an indicator of sprawl: evidence from a Mediterranean urban region. Habitat Int. 38, 119–125. http://dx.doi.org/10.1016/j.habitatint.2012.05.006.

Santamouris, M., 2007. Heat Island research in Europe: the state of the art. Adv. Build. Energy Res. 1, 123–150. http://dx.doi.org/10.1080/17512549.2007.9687272.

Schwarzkopf, M.D., Fels, S.B., 1991. The simplified exchange method revisited — an accurate, rapid method for the computation of infrared cooling rates and fluxes. J. Geophys. Res. 96 (D5), 9075–9096. http://dx.doi.org/10.1029/89JD01598.

Shashua-Bar, L., Hoffman, M.E., 2000. Vegetation as a climatic component in the design of an urban street: an empirical model for predicting the cooling effect of urban green areas with trees. Energy Build. 31, 221–235. http://dx.doi.org/10.1016/S0378-7788(99)00018-3.

Shashua-Bar, L., Tsiros, I.X., Hoffman, M.E., 2010. A modeling study for evaluating passive cooling scenarios in urban streets with trees. Case study: Athens, Greece. Build. Environ. 45, 2798–2807. http://dx.doi.org/10.1016/j.buildenv.2010.06.008.

Shin, H.H., Hong, S.Y., 2011. Intercomparison of planetary boundary-layer parametrizations in the WRF model for a single day from CASES-99. Boundary-Layer Meteorol. 139, 261–281. http://dx.doi.org/10.1007/s10546-010-9583-z.

Sismanidis, P., Keramitsoglou, I., Kiranoudis, C.T., 2015. A satellite-based system for continuous monitoring of surface urban Heat Islands. Urban Clim. 14, 141–153. http://dx.doi.org/10.1016/j.uclim.2015.06.001.

Skamarock, W.C., Klemp, J.B., Dudhia, J., Gill, D.O., Backer, D.M., Duda, M.G., Huang, X.Y., Wang, W., Power, J.G., 2008. A Description of the Advanced WRF Version 3, NCAR Technical Note (NCAR/TN-475 + STR). Boulder, Colorado, USA.

Stathopoulou, M., Synnefa, A., Cartalis, C., Santamouris, M., Karlessi, T., Akbari, H., 2009. A surface heat island study of Athens using high-resolution satellite imagery and measurements of the optical and thermal properties of commonly used building and paving materials. Int. J. Sustain. Energy 28, 1–3. http://dx.doi.org/10.1080/14786450802452753.

Tan, J., Zheng, Y., Tang, X., Guo, C., Li, L., Song, G., Zhen, X., Yuan, D., Kalkstein, A.J., Li, F., Chen, H., 2010. The urban heat island and its impact on heat waves and human health in Shanghai. Int. J. Biometeorol. 54, 75–84. http://dx.doi.org/10.1007/s00484-009-0256-x.

Tewari, M., Chen, F., Wang, W., Dudhia, J., LeMone, M.A., Mitchell, K., Ek, M., Gayno, G., Wegiel, J., Cuenca, R.H., 2004. Implementation and Verification of the Unified NOAH Land Surface Model in the WRF Model. 20th Conference on Weather Analysis and Forecasting/16th Conference on Numerical Weather Prediction. pp. 11–15.

United Nations, 2014. World Urbanization Prospects, The 2014 Revision, Department of Social and Economic Affairs, Population Division, United Nations, New Work. Available online at. https://esa.un.org/unpd/wup/publications/files/wup2014-report.pdf.

Vahmani, P., Ban-Weiss, G.A., 2016. Impact of remotely sensed albedo and vegetation fraction on simulation of urban climate in WRF-urban canopy model: a case study of the urban heat island in Los Angeles. J. Geophys. Res. Atmos. 121, 1511–1531. http://dx.doi.org/10.1002/2015JD023718.

Vahmani, P., Hogue, T.S., 2014. High-resolution land surface modeling utilizing remote sensing parameters and the Noah UCM: a case study in the Los Angeles Basin. Hydrol. Earth Syst. Sci. 18, 4791–4806. http://dx.doi.org/10.5194/hess-18-4791-2014.

Voogt, J.A., Grimmond, C.S.B., 1999. Modeling surface sensible heat flux using surface radiative temperatures in a simple urban area. J. Appl. Meteorol. 39, 1679–1699. http://dx.doi.org/10.1175/1520-0450(2000)039<1679:MSSHFU>2.0.CO;2.

Ward, K., Lauf, S., Kleinschmit, B., Endlicher, W., 2016. Heat waves and urban heat islands in Europe: a review of relevant drivers. Sci. Total Environ. 569–570, 527–539. http://dx.doi.org/10.1016/j.scitotenv.2016.06.119.

Zhao, L., Lee, X., Smith, R.B., Oleson, K., 2014. Strong contributions of local background climate to urban heat islands. Nature 511, 216–219.